Czech Technical University in Prague
Faculty of Nuclear Sciences and Physical Engineering
Department of Nuclear Chemistry

On-line Separation of Cyclotron-Produced Homologues of Transactinide Elements

Bachelor Thesis

Author: Alice Bulíková
Supervisor: Ing. Pavel Bartl
Consultant: doc. Ing. Mojmír Němec, Ph.D.

2022

Acknowledgements

I would like to give my most sincere thanks to my supervisor Ing. Pavel Bartl for generously sharing his knowledge and expertise with me and persistently guiding me through the process with all the patience and support that I have needed.

Declaration

I hereby declare that I have written the bachelor thesis solely by myself under the professional supervision of Ing. Pavel Bartl and that no other sources, other than listed in the references, have been used.

In Prague on .....

.....

Alice Bulíková

Title: On-line Separation of Cyclotron-Produced Homologues of Transactinide Elements

Author: Alice Bulíková

Branch: Nuclear Chemistry

Type of thesis: Bachelor Thesis

Supervisor: Ing. Pavel Bartl
CTU in Prague, FNSPE, Department of Nuclear Chemistry

Consultant: doc. Ing. Mojmír Němec, Ph.D.
CTU in Prague, FNSPE, Department of Nuclear Chemistry

Abstract: Transactinides are artificial elements prepared using nuclear reactions, whose yields tend to be very small and in the combination with very short half-lives of transactinides, the research of the chemical behavior of these elements is challenging in many aspects. Therefore, preliminary experiments are carried out with their lighter homologs. The theoretical part of the thesis describes the synthesis of transactinides and the subsequent approach to study their chemical properties, which is distinctive due to the abovementioned limitations. Apparatuses used to study the chemical properties of transactinides in the gaseous and aqueous phase are described. The thesis is further focused on the synthesis and the study of chemical properties of seaborgium, followed by familiarization with the chemical properties of its homologs – molybdenum and tungsten. In the second half of the theoretical part, there is a description of liquid-liquid extraction, of other chemical systems for the extraction of Sg homologs, and of continuous and microfluidic extraction techniques. At the end, the detection of transactinides, ^{99}Mo and a mixture of cyclotron-produced isotopes of W is discussed. The goal of the experimental part of the thesis is to find a suitable chemical system for the liquid-liquid extraction of seaborgium with the help of its homologs. The aqueous phase of the studied chemical system consisted of HNO_3 in *p*H range of -0.30 - 2.00, while the organic phase contained the extractant Cyanex® 600 in concentrations of 0.007 - 0.70 mol L^{-1} dissolved in kerosene with 1% addition of octanol. Furthermore, an apparatus for microfluidic separation was constructed, which was used for the extraction of Mo by the chemical system described above. The obtained results show that the most effective extraction occurs at *p*H 1.00 - 2.00. As for the concentration of the extraction reagent, it is shown that its increase leads to an increase in *D*-values. From the microfluidic experiments, it can be concluded that the 4-s time of contact, which is suitable for short-lived seaborgium, provides sufficient extraction of Mo with a value of $D = (17.2 \pm 0.2)$.

Keywords: transactinides, homologs, ^{99}Mo, liquid-liquid extraction, microfluidics

Název práce: On-line separace cyklotronových homologů transaktinoidů

Autor: Alice Bulíková

Obor: Jaderná chemie

Druh práce: Bakalářská práce

Vedoucí práce: Ing. Pavel Bartl
ČVUT v Praze, FJFI, Katedra jaderné chemie

Konzultant: doc. Ing. Mojmír Němec, Ph.D.
ČVUT v Praze, FJFI, Katedra jaderné chemie

Abstrakt: Transaktinoidy jsou umělé prvky, které se připravují pomocí jaderných reakcí, jejichž výtěžky bývají velmi malé a v kombinaci s velmi krátkými poločasy přeměny transaktinoidů je zkoumání chemického chování těchto prvků z mnoha hledisek náročné. Proto se uplatňují preliminární experimenty prováděné s jejich lehčími homology. V teoretické části práce je popsána syntéza transaktinoidů a následný přístup ke studiu jejich chemických vlastností, který je vzhledem k výše zmíněným omezením jim typický. Popsány jsou aparatury používané ke studiu chemických vlastností transaktinoidů v plynné a kapalné fázi. Práce je dále soustředěna na syntézu a studium chemických vlastností seaborgia, po kterém následuje seznámení s chemickými vlastnostmi jeho homologů – molybdenu a wolframu. V druhé polovině teoretické části se nachází popis kapalné extrakce, popis dalších chemických systémů pro extrakci homologů Sg, kontinuální a mikrofluidní extrakce. Na závěr je diskutována detekce transaktinoidů, ^{99}Mo a směsi cyklotronových izotopů W. Cílem experimentální části práce je najít vhodný chemický systém pro kapalinovou extrakci seaborgia za pomoci jeho homologů. Vodná fáze studovaného chemického systému se skládala z HNO_3 v rozsahu *p*H -0,30 – 2,00, přičemž organická fáze obsahovala extrakční činidlo Cyanex® 600 v koncentracích 0,007 – 0,70 mol l^{-1} rozpuštěné v kerosenu s 1% přídavkem oktanolu. Dále byla sestrojena aparatura pro mikrofluidní separaci, která byla použita pro extrakci Mo výše popsaným chemickým systémem. Ze získaných výsledků vyplývá, že k nejúčinnější extrakci dochází při *p*H 1.00 - 2.00. Pro koncentraci činidla platí, že jejím zvýšením dochází k zvýšení hodnot *D*. Z mikrofluidních experimentů lze vyvodit závěr, že 4s doba kontaktu, která je vhodná pro krátkodobé seaborgium, poskytuje postačující extrakci Mo s hodnotou $D = (17{,}2 \pm 0{,}2)$.

Klíčová slova: transaktinoidy, homology, ^{99}Mo, kapalinová extrakce, mikrofluidika

Contents

1 Introduction

This work is devoted to fundamental science, which is a field of science often criticized by the general public for being unnecessary. Such a concerning opinion has to be argued with: of course there is a generally approved claim that it builds a platform to better understand the lore of nature and as such it plays an important role in our society and culture. For a stubborn pragmatist, only the vision of practical application stands as a solid argument to defend its purpose. There are many examples in history, where critics of seemingly useless research have been proven wrong.

In the year 1847, George Boole, who was a self-taught scholar interested in the topics of mathematics, logic, and philosophy, published a book titled "The mathematical analysis of logic", where he toyed with the fierce idea of combining mathematics and logic. The discipline was explored by other mathematicians who treated it as a mere curiosity. Nowadays, "Boolean algebra" stands as a foundation for all modern programming languages with Boolean variables of *true* and *false*, denoted 1 and 0, in the foreground. [1]

The search for superheavy elements is a scientific adventure, for which the quote *"It is not about the destination, it is about the journey"* may or may not apply. Is there a limit to the expansion of the Periodic Table of Elements? If so, where does it end and how do we know when we have already reached the end? With each next step and big discovery in superheavy element research, these question are recycled. The common consensus nowadays says we may expect more and more new elements coming. With synthesis of brand-new elements, an opportunity arises to study their physical and chemical properties and as a result expand the range of tools for humanity in the future. To study such universally rare elements is a challenge that one should conquer only when adequately equipped with prior knowledge as not to waste material and human resources.

This work builds on previous research conducted by the Department of Nuclear Chemistry, FNSPE, CTU, which is devoted to the development of one of the possible chemical systems for extraction of molybdenum and tungsten. The elements Mo and W are so-called chemical homologs. Not only they are chemically homologous to one another, but also to a third element, the main focus of the research – a superheavy element called seaborgium. The system should not be steered towards only being the best system to extract Mo and W, but it should firstly be applicable to extraction of seaborgium. Separation of superheavy elements however carries its own specific conditions and restrictions (most importantly low yields and low half-lives).

In the theoretical part of this work an overview will be made about the synthesis, approach to experiments, and chemistry of superheavy elements in the gaseous and aqueous phase. Afterwards, the focus will be put on seaborgium specifically. The reader will be introduced to the synthesis of Sg, gaseous and aqueous chemistry of Sg, as well as the chemistry of its homologs. The liquid-liquid extraction technique will be described and a number of possible extraction chemical systems will be introduced. The problematics of microfluidics will be briefly discussed – its characteristics including advantages and disadvantages. Finally, detection of the isotopes of the abovementioned elements will be brought up, whilst also shedding light on detectors themselves.

In the experimental part of this work (where the chemical system was chosen based on previous experiments) the extractability of Mo and W dependent on *p*H values and extractant concentrations will be explored. The experiments, expected to be conducted with Mo and W separately, will be compared and evaluated. The final part will be putting the explored chemical system into continuous conduct by building an apparatus for continuous extraction, which could be potentially also used in the seaborgium experiments in the future.

2 Transactinides

They are by definition a group of chemical elements with a proton number $Z \geq 104$, currently only theoretically followed by superactinides with $Z > 120$ [2]. At the moment, they are the heaviest elements in the Periodic Table, thus the interchangeable term Superheavy Elements (SHEs) is also used.

Transactinides, subsequent to actinides, can be found in the 7th period, which was completed in 2016 with the official naming of the elements 113, 115, 117 and 118 by The International Union of Pure and Applied Chemistry (IUPAC) [3]. The complete list of transactinides can be found in Tab. 1.

Tab. 1: List of the names, symbols, and proton numbers of transactinides. Adapted from [4].

104 Rf rutherfordium	105 Db dubnium	106 Sg seaborgium	107 Bh bohrium	108 Hs hassium
109 Mt meitnerium	110 Ds darmstadtium	111 Rg roentgenium	112 Cn copernicium	113 Nh nihonium
114 Fl flerovium	115 Mc moscovium	116 Lv livermorium	117 Ts tennessine	118 Og oganesson

All transactinides are highly unstable, as their half-lives are usually in the order of magnitude from milliseconds to minutes (the longest-lived isotope of any transactinide is ^{268}Db with the half-life of 29 h, while the shortest-lived ones reach only microsecond values, e.g. $^{261}Sg^{m}$ with $T_{1/2}$ = 9.3 μs [5]). The lower limit of half-lives is set by one of the criteria for the discovery of a new element that says the lifespan of the synthesized nucleus has to be at least 10^{-14} s, a time needed to form an electron shell around the atom nucleus, which makes it an element with its respective chemical properties [2].

2.1 Synthesis

Transactinides, alike transuranium elements, cannot be found in the nature and must be synthesized artificially through fusion nuclear reactions. The fusion reaction mechanism (see Fig. 1) is based on a bombardment of a target nucleus with a projectile nucleus, where the latter needs to overcome the Coulomb barrier in order for both nuclei to successfully fuse and form a highly excited compound nucleus, which immediately de-excites itself by evaporation of neutrons, in the case it survives. Otherwise, the compound nucleus undergoes spontaneous fission. Each of these individual steps (projectile capture, compound nucleus formation and its survival) happen with a certain probability that is encompassed in the total production cross section.

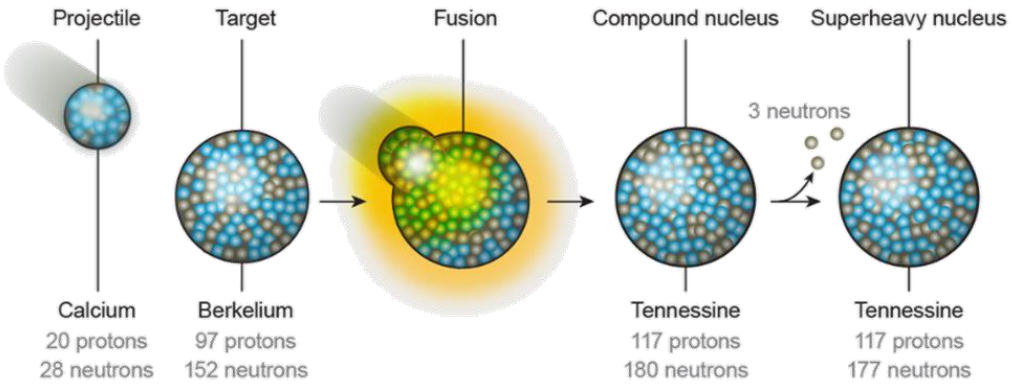

Fig. 1: Mechanism scheme of a fusion nuclear reaction. Adapted from [6].

Fusion reactions are typically divided into hot and cold fusion reactions. Sometimes we can come across the term "warm fusion", which we will regard as a type of a hot fusion reaction [7][8]. The temperature-related categories were dubbed as such based on the excitation energy of the compound nuclei. The excitation energy of a compound nucleus produced in a cold fusion reaction is bounded from above and shall not exceed 20 MeV [9]. In general, higher excitation energies lead to evaporation of more neutrons since one evaporated neutron carries away up to 10 MeV. Therefore, during cold fusion only one or two neutrons are evaporated, whilst in hot fusion method evaporation of 3+ neutrons is expected (Fig. 2).

Hot fusion is the earlier method. It originated as a bombardment of a target made of very heavy nuclei, usually actinides, with light ions ($Z \leq 10$) (e.g. ^{18}O, ^{22}Ne). Then, the projectile Z values were gradually increased (^{26}Mg, ^{34}S, etc.) until later on it was found that ^{48}Ca-induced reactions on actinide targets ($^{242,244}Pu$, ^{243}Am, $^{245,248}Cm$, ^{249}Bk, ^{249}Cf) have some benefits in terms of cross sections. Reactions employing the ^{48}Ca projectiles were grouped into their own subcategory of hot fusion called warm fusion. The warm fusion approach was heavily utilized to discover the heaviest elements 114-118 (Fig. 2). However, synthesis of element 119 and beyond [10] based on this method is challenging and most likely is not going to happen in the near future due to the lack of milligram quantities of heavier actinides, specifically Es and Fm. As a result, scientists use the heaviest actinide target they have access to with a combination of ^{50}Ti beam. Overall, hot fusion method led to the first synthesis of elements 104-106, 112 and 114-118.

Cold fusion leads to a slightly elevated cross section and a decrease of de-excitation energy in comparison to hot fusion. Cold fusion is characterized by the choice of the nuclear target, ^{208}Pb and ^{209}Bi. Heavy ions of ^{50}Ti, ^{54}Cr, ^{58}Fe, $^{62,64}Ni$, ^{70}Zn rich in neutrons are used for the projectiles. The cold fusion reaction was utilized to discover superheavy elements 107-111 and 113.

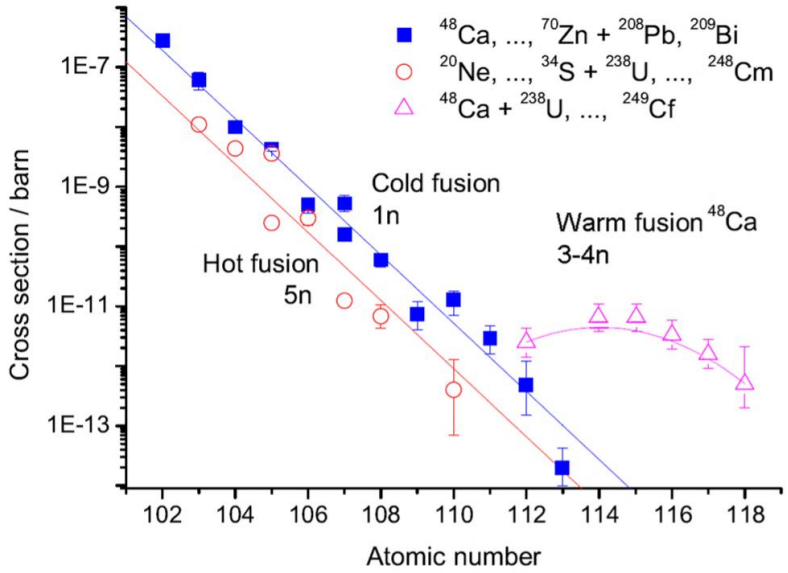

Fig. 2: Experimental cross sections depending on Z for hot, warm, and cold fusion methods. Adapted from [9].

The strong utilization of ^{48}Ca in hot fusion method and ^{208}Pb (and ^{209}Bi) in cold fusion method is not a coincidence. The stable isotope of calcium ^{48}Ca (with abundance of only 0.187 %) has shown to be a promising isotope thanks to its composition. Magic numbers are responsible for its stability and nuclear symmetry. Reaching the magic proton number (2, 8, 20, 28, 50, 82 and unconfirmed 114, 120 or 126) or the magic neutron number (2, 8, 20, 28, 50, 82, 126, 184) has a similar effect in the nucleus as a closed electron shell [12]. With proton number of Z = 20 and neutron number of N = 28, this calcium isotope is "doubly magic" and also rich in neutrons, which helps the newly-formed excited compound nucleus to withstand the neutron evaporation.

The most common isotope of lead is ^{208}Pb, which is also, such as aforementioned ^{48}Ca, doubly magic (Z = 82, N = 126). It is the heaviest stable nuclide. Previously, ^{209}Bi (N = 126) was incorrectly regarded as the heaviest stable nuclide. That was until the year 2003, when its half-life was measured to be $1{,}9 \cdot 10^{19}$ years [13]. Thanks to its neutron magic number and its proximity to be doubly magic, it is also commonly used as a suitable target nuclide for the method of cold fusion.

Being magic is not only an asset associated with projectiles, but the products too. After ^{208}Pb, the next heaviest doubly magic atom has not been synthesized yet. However, with neutron number of 184 and the corresponding proton number so far not known, it is certain to lie in the supposed area of superheavies called the Island of Stability, where the nuclei are predicted to have longer half-lives. Reaching the Island is viewed as a big steppingstone to revolutionize superheavy element research, sadly with no clear path to success in sight [12][14].

2.2 Study of the chemical properties of transactinides

After synthesis, said product is usually to be chemically studied, and ultimately transported to a detection device. The most straightforward, but nowadays an obsolete, method yielding reaction products for further analysis, is *the catcher foil method*, in which a thin foil is placed behind the target to collect the recoiled atoms. This foil is then removed and placed in a detection device or washed for further chemical experiments. The predominantly used method is *the gas-jet transport technique*, where the recoil transfer chamber is connected to the gas-jet transport system, which uses a carrier gas seeded with various aerosol particles (e.g., KCl or carbon), that catch the product atoms and transport them to a manual collection site or an automated chemical device, where its chemical properties are to be studied before being led to a detector for identification. For gas-phase chemistry experiments, aerosols are omitted and pure gas (or mixture of gases) is used instead [15].

The study of chemical properties of transactinides is notorious for pushing the term "trace amounts" to its ultimate limit. The combination of slow rates of production with short half-lives can create marginal situations of only one atom residing in the system. This calls for the utmost care regarding purity, which is achieved by including a gas-filled separator in the set up in between the target and the recoil transfer chamber. The recoiled atoms enter (together with all the by-products that could potentially interfere with the chemistry or detection) into the gas-filled separator, which uses a magnetic field to separate the products [16].

2.2.1 One-atom-at-a-time chemistry

The existence of only one atom in the system does not result only in experimental, but also in theoretical predicaments. Chemical properties are defined by fundamental kinetic and thermodynamic quantities that cannot be freely applied to experimental arrangements consisting of only one atom. Thermodynamic equilibrium constant K_{eq} can serve as an example. Chemical equilibrium of a chemical reaction denoted as

$$\alpha \, \mathrm{A} \leftrightarrow \beta \, \mathrm{B} \tag{1}$$

is a condition in the course of a dynamic reversible process during which reactants A and products B interchange both ways at equal rates so no net change of the composition can be observed over time.

Equilibrium constant is equal to the ratio of the rate constants of the forward and backward reactions k_f and k_b or the ratio of thermodynamic activities of reactants and products {A} and {B} raised to the power of their stoichiometric coefficients α and β:

$$K_{eq} = \frac{k_f}{k_b} = \frac{\{B\}^{\beta}}{\{A\}^{\alpha}} \tag{2}$$

Since thermodynamic activity of substance A relates to its equilibrium concentration [A] and activity coefficient γ as follows:

$$\{A\} = [A] \cdot \gamma \tag{3}$$

then for diluted solutions in stable experimental conditions, K_{eq} can be expressed as:

$$K_{eq} \approx \frac{[B]^{\beta}}{[A]^{\alpha}}. \tag{4}$$

One atom can reside either in one form or the other. That would correspond to equilibrium constant reaching limit values of 0 (atom is in the reactant form) and infinity (atom is in the form of a product) at the time of detection. One of the solutions is to substitute concentrations with probabilities of occurrence of the observed atom in the form of reactant or product.

2.2.2 Experimental approach

For statistical significance an experiment with only one atom must be repeated several hundreds or even thousands of times with a cycle time lasting no more than approximately the half-life of the nuclide under investigation. This time requirement does not affect only the physical parameters of the experimental set-up, but also the choice of the chemical system. The partition method of choice must evince fast kinetics for the equilibrium to be established rapidly. Another complication arises with the unpredictability of the time of creation which causes most of the repeated discrete collections not to contain the desirable product of the reaction at all since it is a common occurrence to produce just one atom in the span of a day or a week. This is why continuous conduct is essential. The whole campaign encompassing synthesis, chemical procedure, and detection of such a number of individuals lasts weeks [8, 9].

2.2.3 Use of homologs for the study of superheavies

The existence of chemical homologs can be exploited in the pursue of finding an ideal separation system for as rare elements as transactinides. Chemical homologs are simply defined as a group of elements that express analogical chemical behavior. Usually, they reside in the same periodic group – therefore, confirming The Periodic Law: when atomic weight is used as the guarding principle to sort elements, similar properties can be periodically observed [18]. The ideal system is identified as the fastest, most efficient, and most specific. The chemical system's conditions are predicted by complicated theoretical mathematical calculations and also practically investigated by running experiments with the corresponding lighter homologs. However, not only preliminary experiments are performed with the lighter homologs. Ancillary experiments are required in order to assure identical experimental conditions to make justified comparisons between the superheavy element and its lighter counterpart. Also, it serves as evidence of an experiment running according to plan, since the low number of registered disintegrations (e.g. only 3 daughter α-α decay chains detected in liquid phase experiment with Sg [19]) is unreliable.

Unsurprisingly, homologs express only resemblance and do not display complete parities of behavior. Therefore, attention has to be paid to the extent of homology. For example, elements $_{104}$Rf and $_{105}$Db are notably deviant from their homological group, whilst $_{106}$Sg, on the other hand, is unconventionally well-behaved [20]. Generally, this deviation from The Periodic Law is caused by relativistic effects, whose impact is growing with increasing atomic weight. With superheavy elements, this effect is significant. These relativistic effects inflict sudden changes in the structure of electron shells, whose deformities can be summarized and simplified as shrinking of spherically symmetric orbitals (*s* and $p_{1/2}$) and expansion of non-spherical (*d* and *f)* orbitals. The slightly altered electronic configuration manifests itself in unexpected chemical behavior [21].

2.2.4 Aqueous phase chemistry of transactinides

Despite the given restrictive conditions, manual experiments were routinely performed, although the reproducibility of the results suffered due to the dependence on speed and endurance of the experimenters. In the occasion when experimental data from manual and automated systems are available, the latter are preferred. Manual separation experiments were done in a discontinuous batch-wise regime using standard chemical procedures, typically liquid-liquid extractions, ion-exchange chromatography, or reversed-phase extraction chromatography [15], [17], [19], [22].

Automated chemistry studies in liquid phase can be executed using a computer-controlled instrumentation system called **ARCA** - Automated Rapid Chemistry Apparatus (also ARCA II and mini-ARCA). It conducts **rapid high-pressure liquid chromatography** column experiments in a discontinuous manner. ARCA II, coupled with an automated on-line α-particle detection system, becomes a system nicknamed AIDA (Automated Ion-exchange separation apparatus coupled with the Detection system for Alpha spectroscopy). ARCA II consists of a central unit – a mobile magazine carrying twenty 8mm × 1.6mm chromatography columns, which allows the system to simultaneously collect activity from a gas-jet transport system (He, KCl) on a frit, carry out the experiment, and prewash and condition the columns. The flow rate in the columns can be set in a range from 0 to 10 mL min^{-1}.

A full cycle is done within 30 s. Whilst the chemistry investigation is carried out, the preparation of the sample for α-spectroscopy has to start already. Droplets are collected on a hot (99 °C) tantalum plate, where they are targeted by a source of NIR light (tungsten filament) and hot helium gas. Once the sample volume of 100 μL is evaporated to dryness, the disc is cooled by liquid nitrogen to room temperature and can be transferred to a detector [23].

The **SISAK** apparatus is both an automated and a continuous microcentrifuge system for performing **liquid-liquid extractions**. SISAK III, developed in 1989, consists of static mixers and mini centrifuges to separate phases and can be applied on radionuclides with half-lives of 1 s and up. The flow rate can be varied from 0.1 up to 3 mL s^{-1} per phase. The most significant drawback of any generation SISAK is the relatively high flow rate, which creates substantial amounts of liquid waste. Thus, a miniaturized device has been developed – MicroSISAK, a micro membrane extractor with micromixers and a hydrophobic membrane for separation, which operates at flow rates of around 0.2 mL min^{-1} for both phases [24], [25].

All the processing systems mentioned above function based on partition processes, thus distribution constant K_D, introduced in chapter 1, is obtained. Other characterizations of superheavies, that can also be acquired with chemical experiments in liquid phase, are ionic radii, ability to form chemical compounds, complex formation, hydrolysis, and redox potentials (valence electronic states) [19].

Aqueous phase chemistry was investigated only for three transactinides: Rf, Db and Sg. [19] A detailed description of the chemical behavior of seaborgium in aqueous phase can be found in chapter 3.2.1.

2.2.5 Gas phase chemistry of transactinides

Only a few inorganic compounds of transactinides exist that are volatile below the experimentally feasible temperature of 1000 °C. Despite that, gas phase chemistry experiments are widely utilized mostly thanks to their speed, efficiency, and convenience of being performed in one phase. The recoiled atoms usually travel through a gas-filled separator to a recoil transfer chamber, where they are thermalized. The chamber is directly connected with a thin capillary to a gas chromatographic system. Two types of gas chromatography methods can be implemented: isothermal chromatography and thermochromatography [26].

In isothermal chromatography, the temperature throughout the chromatography column is kept constant. The carrier gas has a constant flow; yet different species travel downstream at varied speeds. The retention time of the studied species depends on the temperature in the column and more significantly also on the enthalpy of adsorption of the molecule on the column surface ΔH_{ads}, which means less volatile species are retarded more. During the experiment, the temperature is continuously isothermally increased in order to track yields and to determine $T_{50\%}$. At the temperature of $T_{50\%}$, half of the introduced nuclides emerge at the end. The retention time is then equal to the half-life of the radionuclide [11], [26].

In thermochromatography, a negative longitudinal temperature gradient is applied to the chromatography column using a thermostat at the head of the column and a liquid nitrogen cooling system at the exit. Aided by the carrier gas, the more volatile species are carried further down the length of the column where they deposit. The place of deposition (with temperature T_a) is identified by a strip of detectors for alpha and spontaneous fission decay placed along the track [11].

An automated gas analyzer system called **OLGA** (On-Line Gas Chromatography Apparatus) utilizes the isothermal chromatography technique. A gas-jet transport system helps to transport the products to a chromatography system in less than 10 s. In the first-generation apparatus, the separated products were condensed on thin metal foils on a rotating plate and moved to a detector. This detection system is called ROMA (Rotating wheel Multidetector Analyzer). In OLGA II, a new technique called reclustering was introduced. Reclustering is a process of re-attaching the separated species to new aerosol particles, which are then carried via a capillary directly into a detector. OLGA III and an improved version of OLGA from Berkeley nicknamed **HEVI** (Heavy Element Volatility Instrument) are upgraded systems in terms of chromatographic resolution and speed of separation [11].

Chemistry in gas phase was investigated for distinctly more elements than aqueous chemistry. Specifically, elements 104, 105, 106, 107, 108, 112, 113, 114 [26] and 115 [27].

3 Seaborgium

Seaborgium (Sg), the 106th chemical element of the Periodic Table and 3rd lightest transactinide, can be found in group 6. It is predicted to be a transition metal solid at room temperature. The electron configuration for seaborgium should be [Rn] $7s^2\,5f^{14}\,6d^4$ with experimentally confirmed oxidation states of 0 and 6, whilst oxidation states of 3, 4 and 5 are being predicted.

3.1 Synthesis of Sg

As a synthetic element it does not naturally occur in the Earth's crust. It was first synthesized in 1974 by Lawrence Berkeley Laboratory lead by Albert Ghiorso in Berkeley, California. They utilized a hot fusion reaction of target ^{249}Cf in collision with ^{18}O accelerated using Super-Heavy Ion Linear Accelerator (Super HILAC). The produced nuclide was determined to be ^{263}Sg, which underwent alpha decay to ^{259}Rf, which was also susceptible to alpha decay to ^{254}No as described in the equation below.

$$^{263}Sg \xrightarrow{\alpha} {}^{259}Rf \xrightarrow{\alpha} {}^{254}No \tag{5}$$

Three months prior to their announcement a group of scientists from Joint Institute for Nuclear Research in Dubna, U.S.S.R., reported the same discovery. Using an innovative cold fusion reaction with target nuclides of Pb 206, 207 and 208 colliding with cyclotron-accelerated projectiles of ^{54}Cr, a nuclide ^{259}Sg was apparently formed.

The work of the Lawrence Berkeley Laboratory team was confirmed only in 1993, when they were credited for their discovery after providing sufficient indisputable evidence including the record of successive alpha decay chains and earned the privilege of suggesting a name for the element, which resulted in another controversy as honoring a living person seemed unthinkable. The situation was resolved in 1997 by IUPAC. The newly discovered element was named after Glenn T. Seaborg (1912-1999), a Chemistry Nobel Prize winner, who discovered and investigated a number of transuranium elements and played a significant role in forming the Periodic table we know today. This set a precedent in naming new elements. The element 118 carries the name of another living eponym Yuri Oganessian, a leading researcher in the field of superheavies and inventor of the cold fusion method.

By 2020, 16 isotopes and 6 isomers of Sg have been synthesized [5]. It is important to note that the nuclides are not always synthesized directly; oftentimes, they occur in the decay chain of other superheavies. The most stable isotope of seaborgium is ^{269}Sg with its half-life of 14 minutes [28].

3.2 Chemistry of Sg

Seaborgium chemistry experiments were carried out both in an aqueous and a gas phase. All of them confirmed its group-6-element behavior, aligning with the behavior of the chemical homologs molybdenum and tungsten. Other than to confirm the placement in the Periodic Table of Elements, studies are performed to study the formation and properties of its compounds [21]. The most relevant compounds that seaborgium forms are oxides, halides, oxohalides, hydroxohalides and carbonyls [22].

3.2.1 Aqueous phase chemistry of seaborgium

In the beginning, theoretical mathematical calculations predicted a complete analogy between hexavalent elements M = (Mo, W, Sg) for the oxohalide MO_2X_2., where X = (F, Cl). From these theoretical predictions was concluded that the analogical behavior of these homologs could be also experimentally observed in aqueous complexes $[MX_n]^{6-n}$ or $[MO_mX_n]^{6-2m-n}$ formed in HX solutions [17]. The first aqueous-phase experiment was executed by Shädel et al. [29] in 1995 at GSI Helmholtz Centre for Heavy Ion Research, Darmstadt, using UNILAC (The UNIversal Linear Accelerator) and the ARCA II chemistry system equipped with cation-exchange resin chromatography column [22]. The nuclide-loaded aerosols were dissolved in 0.1M HNO_3/$5\cdot10^{-4}$M HF, a solution confirmed in preliminary experiments with Mo and W to provide optimal conditions for separation from di- and trivalent actinides and group-4 elements (that form during Sg preparation), which are retained in the column, while Mo, W and Sg are eluted as under these conditions they do not form positively charged complexes. [11].

The isotope ^{265}Sg was intended to be used, but actually a mixture of 9-s ground and 15-s metastable isomers was present during the experiment, which was unknown at the time. The passage of the compounds through the chemistry set-up takes considerably longer than that, thus the detection of alpha-alpha decay chains of the daughter ^{261}Rf and granddaughter ^{257}No had to suffice as evidence. During 3900 separations with a cycle of 45 s, three of these alpha decay chains were observed [19].

The conclusion of this experiment was that seaborgium elutes from the column just like its homologs and behaves like a typical group 6 element. Depending on the HF concentration, hexavalent anionic or neutral complexes MO_4^{2-}, MO_3F^-, MO_2F_2, $MO_2F_3^-$, $MO_2F_4^{2-}$, MOF_5^- are formed. In the particular case of Sg, either SgO_3F^-, $SgO_2F_3^-$ or $SgO_2F_4^{2-}$ had to be formed. It was also noted, that in order to reach these anionic species, molybdenum or tungsten require higher HF concentrations than seaborgium. The formation of "seaborgate" SgO_4^{2-} and the neutral complex SgO_2F_2 cannot be excluded. The most important finding was that no seaborgyl cations SgO_2^{2+} were formed in the 0.1M HNO_3/$5\cdot10^{-4}$M HF mixture, demonstrating that seaborgium differs from its hypothetical pseudo-homolog uranium [30], which forms uranyl ions UO_2^{2+} and gets fixed in the cation exchange column [11].

The follow-up experiment was performed by the same research group a year later, in 1996, using the same equipment. It was designed to confirm or disprove the formation of seaborgate ions SgO_4^{2-}. The liquid chromatography mobile phase only consisted of 0.1M HNO_3 and the potential complexing agent HF was omitted. Due to its absence, no Sg was eluted, proving that fluorine anions F^- indeed contributed to complex formation and thus no complexes interfered with the study of the specific compound SgO_4^{2-}, which was not detected. The possible explanation is the weaker tendency of Sg to hydrolyze compared to its homologs Mo and W. Under these experimental conditions, Mo and W hydrolyze as far as to reach neutral species $MO_2(OH)_2$, Sg supposedly stops its hydrolysis already at cationic species, such as $SgO_2(OH)^+$, which sorb on the cationic exchange column. [19]

3.2.2 Gas phase chemistry of seaborgium

To perform chemistry experiments in the gas phase, a compound that is satisfyingly volatile and stable is needed. Seaborgium in the elemental state should be extremely refractory, but forms halides, oxyhalides, oxides, oxide hydroxides, and carbonyls, which can be used in gas phase experiments [22]. Halides and oxyhalides are of similar volatility, but a trend in stability can be observed: $SgCl_6 < SgOCl_4 < SgO_2Cl_2$. Oxides and oxide hydroxides of Sg are only moderately volatile, but analogical compounds of Rf and Db are not, which makes them suitable for gas-phase separation experiments. Carbonyls are regarded to be both very volatile and stable [26].

Isothermal gas chromatography was performed using the on-line automated system OLGA III to study compounds SgO_2Cl_2 and $SgO_2(OH)_2$. Specifically, to study their formation and volatility. The substance was formed in a reaction oven filled with chlorinating agents (Cl_2) saturated with $SOCl_2$ and traces of O_2. The adsorption enthalpy was determined. The volatility of the compound MO_2Cl_2 for the elements of group 6 is following: $MoO_2Cl_2 > WO_2Cl_2 = SgO_2Cl_2$. Another acquired information is that seaborgium formed this species typical for group 6 elements and differs from its pseudohomolog U, which forms UCl_6 [22].

Gas phase experiments were also done using the thermochromatography technique. It was observed that firstly SgO_2Cl_2 and WO_2Cl_2 were formed, but WO_2Cl_2 was later converted to the more volatile $WOCl_4$, whereas the ^{263}Sg has already decayed. This unfortunately meant that no relative comparison of seaborgium with tungsten could have been done, as the half-lives were too different and the two species of the respective oxyhalides were present. [26].

Experiments with carbonyls also yielded significant results. The synthesis of the hexacarbonyl required high pressure and temperature between 20 and 200 °C. The apparatus used was the Cryo-Online Multidetector for Physics And Chemistry of the Transactinides (COMPACT), which is a gas-

thermochromatography column and a detector. Experiments with Mo and W were run before and parallel to the Sg experiments, thus direct comparisons could be done. In conclusion, adsorption enthalpies were experimentally determined and confirmed the theoretical predictions. The measured adsorption enthalpies ΔH_{ads} on the SiO_2 surface for ^{87,88}Mo, ^{164}W and ^{265}Sg are, respectively, as follows: 50 ± 2, 49 ± 2 and 50 ± 4 kJ/mol [31].

4 Homologs of Sg and their preparation

Seaborgium is a group 6 element. The other group 6 elements are chromium (Cr), molybdenum (Mo), and tungsten (W), which makes them potential candidates for chemical homology. Molybdenum and tungsten are known for their similar chemistry [32]. Chromium, however, expresses slightly different chemical behavior, that can be illustrated using the most stable oxidation states. Almost all naturally occurring chromium is in the trivalent state (and only in the more unusual environments other oxidation states can be found) [33]. For Mo and W, the most stable oxidation state is +6. Experiments with seaborgium have already shown its resemblance with Mo and W. Chromium is therefore not a suitable chemical homolog [21].

Molybdenum is the lightest practically used homolog of seaborgium. A technetium generator can be used as a molybdenum source, although its primary use is in medical diagnostics and palliative care. It is an ion exchange chromatography column in which the parent nuclide ^{99}Mo is anchored by ionic forces to an alumina stationary phase. The half-life of ^{99}Mo is 66 h and its daughter nuclide ^{99m}Tc has a half-life of 6 h [5]. This disproportionality of half-lives has a specific decay kinetics, which leads to a transient decay equilibrium. Technetium is not held up in the column and can be freely eluted with physiological saline solution. After the elution, the system is misbalanced and it takes about 10 daughter half-lives to recover the equilibrium. Nuclide generators are used as a source for short-lived nuclides, such as ^{99m}Tc since they cannot be kept isolated for reasonably long periods of time. The desirable product, the parent nuclide ^{99}Mo, can be eluted from the generator with an ammonium hydroxide solution [34]. Mo can be also cyclotron-produced, but such preparation technique is more expensive and yields much lower activities compared to ^{99}Mo/^{99m}Tc generators.

Tungsten is not only the heavier homolog, but the suitability for the experiment is further enhanced when the atoms of tungsten are acquired through nuclear reactions to mimic the experimental conditions of transactinide synthesis. These nuclides can be cyclotron-produced using a Hf target and ^{3}He projectiles. Natural hafnium consists of an isotopic mixture of at least 5 stable and 1 long-lived isotope [35]. Besides the nuclear target consisting of an isotopic mixture, an unknown number of neutrons is evaporated. A safe estimate of evaporated neutrons would be a wide range between 1 and 7, where the values of cross section of the outer reaction channels decrease (forming a bell curve), as cross section

(probability of a specific reaction taking place) is subject to normal distribution. The complex process can be described by a generalized nuclear reaction leading to a complicated mixture of tungsten isotopes:

$$^{174,176,\ldots,180}\mathrm{Hf}\ (\ ^{3}\mathrm{He}\ ,\ x^{1}\mathrm{n}\ )\ ^{(177-x),(179-x),\ldots,(183-x)}\mathrm{W} \qquad (6)$$

The final composition of the measured samples can be simplified with some thoughtful assumptions based on information provided in Fig. 3. ^{174}Hf can be omitted for its low abundance. The lightest isotope is then ^{176}Hf which upon fusion with ^{3}He forms ^{179}W evaporating at most c. 7 neutrons coming down to ^{172}W. The heaviest present isotope is ^{180}Hf which is transformed to ^{182}W in case one neutron evaporates. Working with the range of tungsten nuclear numbers of 172 up to 182, we can eliminate tungsten 180 and 182 for being stable, 178, 179 and 181 for not providing any or any sufficient gamma lines and 172 together with 173 for a rather short half-life. Presumably, tungsten-174, 175, 176, and 177 are suitable candidates for liquid-liquid extraction experiments and subsequent HPGe detection.

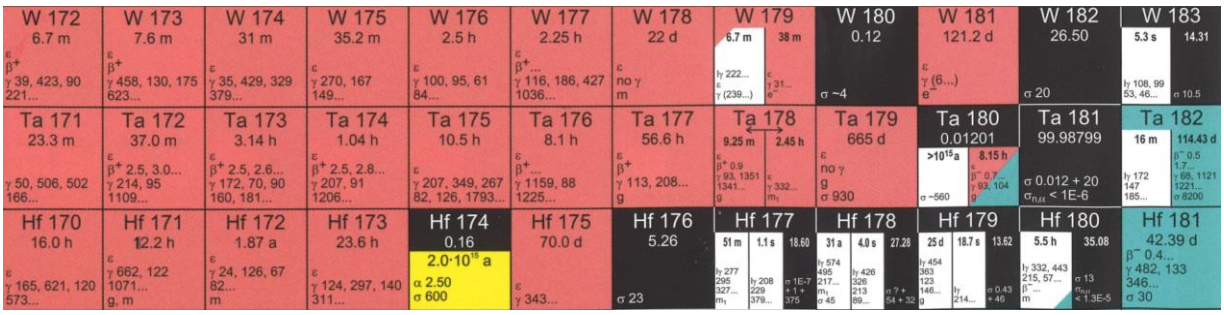

Fig. 3: Cutout of Hf and W isotopes from a nuclide chart. Adapted from [36].

4.1 Aqueous phase chemistry of Mo and W

Molybdenum and tungsten express a rather complicated liquid phase chemistry. Molybdenum has 6 oxidation states: 0, +2, +3, +4, +5, and +6. In aqueous solutions the one most commonly found is the oxidation state +6. When reduced in slightly acidic or neutral solutions, molybdenum (III) (molybdenum blue) is produced, although it is highly susceptible to air oxidation. Molybdenum (V) has to be stabilized by a complexing ion in order to not oxidize [37].Tungsten is analogical to molybdenum in its oxidation state prevalence [32]. From now on, only hexavalent states will be considered as it is the most stable form and no redox processes take place in the extraction systems employed in the experimental part. Further simplification stems from working with (sub)tracer amounts, which makes the formation of polymeric compounds negligible, and thus only monomeric species will be considered.

The two most prominent processes, that the molybdenum or tungsten cations (denoted M) can undergo in aqueous solutions, are hydrolysis and complexation.

4.1.1 Hydrolysis

Both metal cations tend to hydrolyze in water solutions, which means they form coordination compounds with hydroxyl donor ligands. The speciation form is dependent on the *p*H of the solution: acidic solutions promote cationic forms, whilst basic solutions provide the environment for anionic species formation. Equation (7) illustrates a stepwise hydrolysis process as *p*H increases:

$$MO_2^{2+} \rightleftharpoons MO_2(OH)^+ \rightleftharpoons MO_2(OH)_2 \rightleftharpoons MO_2(OH)_3^- \rightleftharpoons MO_4^{2-} . \quad (7)$$

Uniformity regarding denotation is poor as one species may be identified by a number of different formulas. In our case, coordinated water molecules were omitted completely, although it might not depict the molecule accurately [38][39].

4.1.2 Complexation

Because the presence of F^- or Cl^- anions (denoted X^-) is a typical occurrence during experiments with transactinides and their homologs, it is important to remark the strong affinity of molybdenum and tungsten towards halide anions. An analogy can be drawn between hydrolysis and halide complexes: a tendency for anionic species grows with higher concentrations either of OH^- or X^- anions in the solution. Equation (8) shows a stepwise complexation process as concentration of halide anions increases:

$$MO_4^{2-} \rightleftharpoons MO_3X^- \rightleftharpoons MO_2X_2 \rightleftharpoons MO_2X_3^- \rightleftharpoons MO_2X_4^{2-} \rightleftharpoons MOX_5^-. \quad (8)$$

Water molecules were again omitted from the formulas [40].

5 Liquid-liquid extraction

Liquid-liquid extraction (LLE) is a separation method, during which the extracted substance is partitioned between two immiscible liquids. This physicochemical process is based on different solubility of the extracted substance in each of the liquids. The most conventional choice of liquids for a partition system is an aqueous solution (containing the solute) in combination with an organic solution. Other options include melted metals, non-metals, and salts [41] or liquid salts at room temperatures, which are more commonly referred to as ionic liquids (IL). Currently, there is a growing popularity of their implementation in chemical experiments with homologs of transactinides [42], [43].

The fundamental quantity used to describe the partitioning of the substance between two liquids is called the Nernst distribution constant (or partition ratio), denoted K_D. By definition, the distribution constant equals to the ratio of concentration of a substance in a single definite form A in the extractant to its concentration in the other phase. These two phases constitute of two immiscible solvents, e.g., aqueous/organic phase system for liquid-liquid extraction. It should be noted that under isothermal conditions K_D is independent on the total concentration of the substance A.

$$(K_D)_A = \frac{[\mathrm{A}]_{org}}{[\mathrm{A}]_{aq}} \tag{9}$$

In case of working with (sub)tracer amounts, radioactivity of each phase can be considered instead. The equation is as follows:

$$K_D = \frac{A_{org}}{A_{aq}} \cdot \frac{V_{aq}}{V_{org}}, \tag{10}$$

where A and V are activity and volume of a corresponding liquid phase.

Unfortunately, the distribution constant does not allow the complete analytical assessment of an extraction system of a solute with more than one definite form, unless all the definite forms are known or the solute does not interact with any other substance in the system. The latter situation is quite rare, since extraction reagents are often employed for an efficient separation process. For such cases, a distribution ratio or a distribution coefficient, D, is implemented. The distribution ratio describes the total partitioning of the studied substance between the two phases, regardless of its chemical form; thus it is equal to the ratio of the total analytical concentration of a substance A in the organic phase to its total analytical concentration in the aqueous phase:

$$D = \frac{\mathrm{c}_{A,org}}{\mathrm{c}_{A,aq}}. \tag{11}$$

The substance A may exist in the solution in multiple chemical forms (species), whose extractability varies. Analytical concentration can be expressed as a sum of the total concentrations of all the species of the substance A and equation (11) transforms into:

$$D = \frac{\sum_i [A_i]_{org}}{\sum_i [A_i]_{aq}}. \tag{12}$$

In practice, a percentage of extraction, noted *E*, is sometimes used. Simply, it says what percentage of the total amount of the substance is transferred from the aqueous to the organic phase. Its relation to the distribution ratio is expressed as follows:

$$E = \frac{100 \cdot D}{D + \frac{V_{aq}}{V_{org}}}, \tag{13}$$

where V_{aq} and V_{org} are the volumes of the aqueous, resp. organic phase. If E > 99 %, the analyte is said to be extracted "quantitatively". On the other hand, if E < 1 %, then the analyte is not being extracted [41].

To transition from aqueous to organic phase, a substance has to be of a neutral charge or at least a part of its molecule has to be of hydrophobic nature. Some elements (e.g. sulfur, selenium, halogens, and noble gases), oxides (e.g. OsO_4, RuO_4), covalent halides (e.g. AsX_3, SbX_3, GeX_4, SnX_4, HgX_2, BiX_3), etc., are extractable. Metal salts are in its essence unextractable because of their high solubility in water. To extract metal cations, one of the two main manipulation methods has to be employed: formation of ionic associates or complexation (chelation) [41].

The formation of **ionic associates** is an extraction mechanism during which the metal ion (usually complex) associates through attractive electrostatic forces with a provided ion of opposite charge to form a neutral unit (no chemical bonds are formed). This unit is hereafter easily extractable into non-polar solvents [41].

Chelation is an extraction mechanism during which a metal cation M^{n+} reacts with a multi-donor base, typically a deprotonated acid. The water molecules surrounding the hydrated metal cation are displaced and new chemical bonds are formed. The interaction yields a very stable cyclical compound, a type of coordination compound called metal chelate. The process can be described as:

$$\mathrm{M^{n+}} + n(\mathrm{HA})_{\mathrm{org}} = (\mathrm{MA}_n)_{org} + n\mathrm{H^+}. \tag{14}$$

5.1 The influence of condition changes on the extraction of chelates

During separation processes, it is always beneficial to not only know how to encourage the coveted extraction process, but also how to inhibit the extraction of the interfering substances. The extraction of chelates can be impacted by a number of factors, from which only a few will be elaborated on below.

5.1.1 Extraction of chelates as a function of *p*H

The equilibrium *p*H of the aqueous phase (after phases were contacted and equilibrium state was created) is one of the most important parameters to influence the extraction process. Dependence of the percentage of extraction *E* on *p*H forms a characteristically sigmoid "extraction S-curve". At $pH_{1/2}$ is E = 50 %. The difference in $pH_{1/2}$ values of two metal ions illustrates the ease of their mutual separation. The steepness of the slope depends upon valence number *n* in M^{n+} [44]. All abovementioned is depicted in Fig. 4.

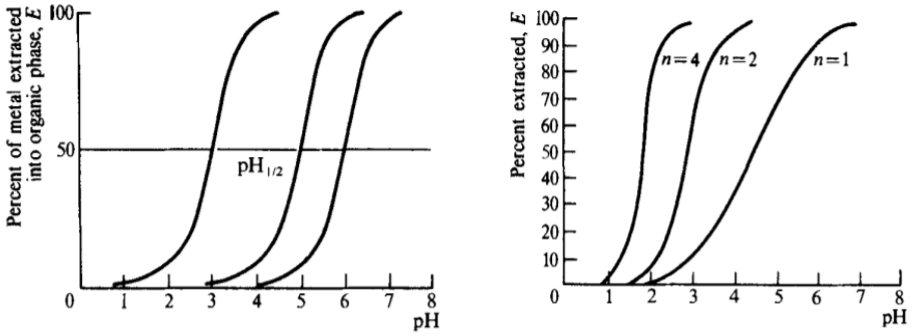

Fig. 4: Sigmoid extraction curves for different metal ions (left) and for metal ions of different valency (right). Adapted from [44].

5.1.2 Extraction of chelates as a function of concentration of extractant

By adjustment of extractant concentrations, the sigmoid extraction curve is shifted horizontally. Higher extractant concentrations lead to improved extractions at lower pH as seen in Fig. 5.

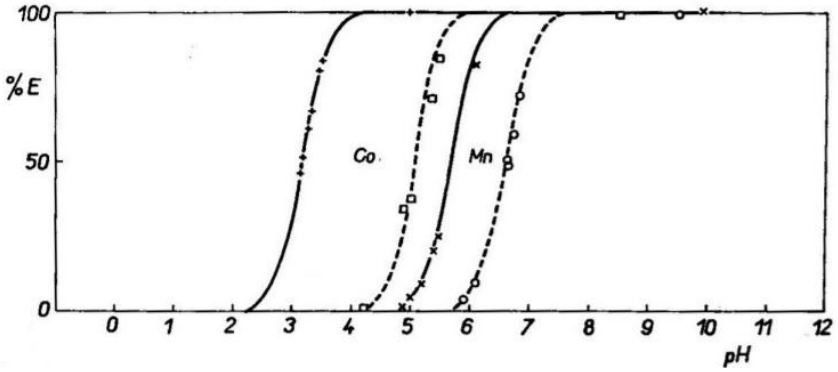

Fig. 5: Extraction of Co(II) and Mn(II) in 0.1M (solid line) and 0.01M (dashed line) solution of 8-hydroxychinoline in chloroform. Adapted from [41].

5.1.3 Influence of the organic solvent on the extraction of chelates

As a general rule, the higher the solubility of an extractant in the organic solvent, the higher the solubility of the formed chelate and therefore improved extractability is expected [41].

5.1.4 Influence of kinetic factors on the extraction of chelates

The rate of reaching extraction equilibrium is dependent on two factors:

1. the rate of the chelation reaction
2. the rate of transfer of the chelates between the two phases.

The former is usually the more time-consuming process, which can take minutes, whilst the transfer happens in order of seconds [34]. Hence, optimization of a chemical system for partition experiments with short-lived radionuclides does not only consider extraction yields, but also kinetic speed is an important variable.

5.2 Extraction systems for Mo, W (and Sg)

The first parameter to consider in search for the extraction system is the amount of the to-be-extracted substance. Extraction of molybdenum or tungsten in the context of them being a superheavy element homolog will be intentionally performed in a subtracer scale to mimic the scarce-element behavior accurately. Since trace amounts are prone to non-negligible sorption on surface areas, acidic environments are preferred as they suppress this effect. In macro amounts, alkaline solutions to extract molybdenum or tungsten are standard (e.g. molybdenum (VI) extraction from NaOH solution by Aliquat 336 mixed with kerosene [45]). For the aqueous phase, a solution of a mineral acid is expected (e.g. HCl, HF, HNO_3, H_2SO_4, H_3PO_4, or combinations are possible), while the second phase consists mostly of an organic solvent (kerosene, toluene, benzene, dodecane, chloroform, …) sometimes enhanced with additives such as a phase modifier. In any case, it must contain the key component: the extracting agent. Molybdenum or tungsten can be extracted using, for example, amine-based extractants, neutral organophosphorus compounds or organophosphorus acids.

Amine-based extractants are classified into categories based on how many hydrocarbon groups are bonded to the nitrogen atom: primary, secondary, tertiary, and quaternary amines. For Mo or W extraction purposes, secondary amines can be used, such as DOA (dioctylamine) or DIDA (diisododecylamine), tertiary amines like TOA (trioctylamine) or Alamine 336 (tricaprylamine) and quaternary ammonium salts like Aliquant 336 (tri-octyl/decyl-ammonium chloride) and TOMAC (tri-n-octylmethylammonium chloride) [46]–[50]. The extraction mechanism they employ is formation of ionic associates.

Another category utilizing this mechanism is the **neutral organophosphorus compounds**, e.g. TBP (tributyl phosphate) and TOPO (trioctylphosphine oxide) [51].

Organophosphorus acids are derivatives of phosphinic (I), phosphorous (III) or phosphoric (V) acid. The dialkyl variants are the most commonly used, which tend to only dimerize, not polymerize like monoalkyls would. They are used as a chelating agent – employing chelation as the extraction mechanism [41]. **DEHPA**, or also noted **HDEHP**, (Fig. 6) is used in both macro and tracer scale extractions of Mo or W.

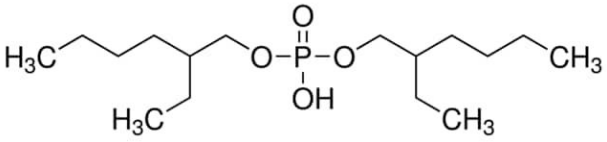

Fig. 6: Chemical structure of DEHPA: bis(2-ethylhexyl)phosphoric acid. Adapted from [52].

In the experimental part of this work, **Cyanex® 600** was used as the extractant of choice**.** It is specifically developed for extraction of molybdenum from acidic solutions. Trademarked by Cytec Industries Inc., it is an industrial extractant with an unknown composition. Supposedly, it is regarded as a dialkyl phosphinic acid with a similar structure to (or the same structure as) **Cyanex® 272** (portrayed on Fig. 7) and enhanced with some phase modifying components.

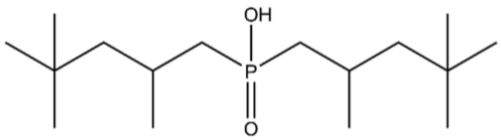

Fig. 7: Chemical structure of extractant Cyanex® 272: bis(2,4,4-trimethylpentyl)phosphinic acid. Adapted from [53].

Reflecting on chapter 4.1.1, MoO_2^{2+} and $MoO_2(OH)^+$ are presumably the two most represented species of molybdenum in the *p*H region of our interest. Let x depend on the degree of protonation, then the mechanism of extraction in a chemical system with extractant Cyanex 600 (HCy) can be described by the equation:

$$\mathrm{MoO_2(OH)_x}^{2-x} + 2 \cdot \mathrm{HCy} \leftrightarrow \mathrm{MoO_2(Cy)_2} + (2-x) \cdot \mathrm{H^+} + x \cdot \mathrm{H_2O}, \tag{15}$$

where x = 0 or 1. This prediction is made using similarities between HDEHP, Cyanex® 272, and Cyanex® 600 [54].

5.3 Continuous extraction

Liquid-liquid extractions are routinely done manually in a batch-wise manner. This accounts for standard radiochemistry and the initial radiochemistry experiments with transactinides as well. As nearly the end of the Periodic Table is experimentally explored, the demands for automatization and continuity grow as the half-lives get shorter and yields of reactions smaller. This forces the number of performed cycles climb to several thousand.

5.4 Microfluidic extraction

Microfluidic extraction is a miniaturized liquid-liquid extraction that deals with small volumes of micro- down to seemingly impossible atto- liters. Such volumes require specialized equipment, e.g. channels with dimensions in the order of hundreds of micrometers at most [55].

5.4.1 Advantages and disadvantages of microfluidics

Microfluidic techniques are convenient for radiochemistry experiments, where disproportionate waste production is especially inadequate. Reagent consumption is concurrently also diminished. This is not only beneficial from waste-of-resources point of view, but a requirement in situations in which unnecessary dilution of a critically small amount of analyte is not welcome. Other advantages of scaling down are more efficient heat dissipation, increased effective interface area thanks to larger surface-to-volume ratio for smaller liquid drops, and an ability to control mixing due to the exploitation of laminar flows typical for micro scales [55]. Microfluidic systems offer easy modularity and automatization, and thereafter utilization in on-line experimental setups. Their compactness is a welcomed bonus.

The disadvantages encompass the pronounced influence of chemical and mechanical impurities, pressure changes, and dead volumes. The unique manifestation of hydrodynamic processes typical for micro scale may impose a challenge too.

5.4.2 Mass transfer and interfacial surface

The intention of microfluidic extraction, or for that matter any other separation method, is to achieve the maximum mass transfer. What affects mass transfer the most, apart from the applied chemical system, is the contact surface between the two phases, which is referred to as an interfacial area. Let us assume a spherical unit of one fluid (a drop) surrounded by the second immiscible fluid. A sphere of radius r has a surface of $4\pi r^2$ and a volume equal to $\frac{4}{3}\pi r^3$, hence the surface to volume ratio of a sphere is inversely proportional to $3r$. Interfacial area is positively affected by the decrease in size of such a sphere. Conclusively, the focus should lie on thorough mixing.

5.4.3 Mixing of the phases

In liquid-liquid extractions, mixing can be done manually in a separatory funnel or in various kinds of vortex, platform, or orbital shakers. All aforementioned are effective techniques of mixing, that can even lead to complete dispersion and formation of an emulsion.

In microfluidic liquid-liquid extractions, contacting of phases happens in a capillary with a characteristic flow regime (or pattern) that allows a certain amount of effective interfacial surface. Flow regimes may be adjusted and a high degree of control over the system is gained. The flow regimes are generated by crossing of two immiscible phases into one channel. This takes place in a mixing zone that can have different geometries (e.g. using T or Y junctions, as pictured on Fig. 8).

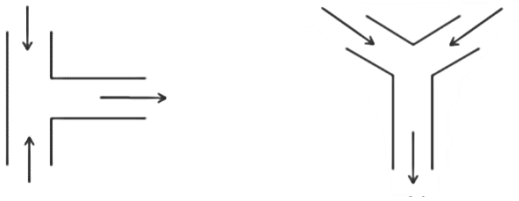

Fig. 8: Schematic of a mixing zone with a geometry of T (left) and Y (right).

To predict a flow pattern is nearly impossible as there are too many variables: flow rate, pressure drop, physical properties of the phases (viscosity, density, surface tension, etc.) and channel properties (dimensions, material, wettability, roughness, etc.) and many more. Some of the flow patterns may be seen on Fig. 9.

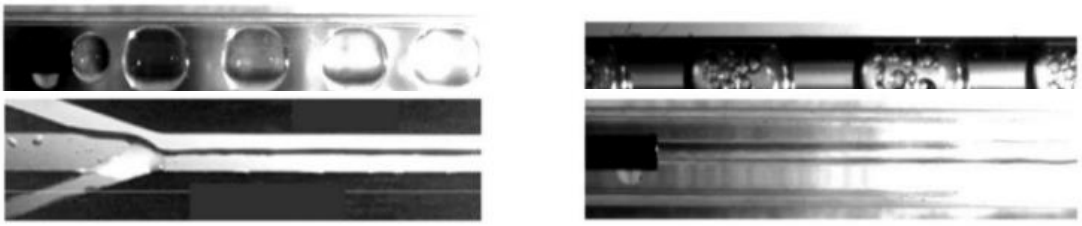

Fig. 9: Photos of a segmented (plug) flow (top left), plug-dispersed flow (top right), parallel flow (bottom left) and annular flow (bottom right). Adapted from [56].

5.4.4 Phase separation techniques

After the phases have been sufficiently contacted, they need to be separated into pure phases with no traces of the other. Phase separation based on density difference is not applicable as capillary, viscous, and convective forces dominate. Fortunately, the two immiscible phases are deemed to display contradictory properties, i.e. hydrophilicity and hydrophobicity utilized in hydrophilic/hydrophobic membrane separation technique. For separation of co-current flow, a simple Y-splitter suffices. Capillary forces and wettability are also exploited in other separation techniques. A comb separator utilizes the former property, whilst a needle separator relies on the latter [57], [58].

5.4.5 Microstructured devices

Miniaturization and compactness have shown to be very convenient and could actually cut costs in the long run. The established name “lab-on -a-chip system” is no exaggeration. Such a system, equipped with injector, transporter, preparator, mixer, reactor, separator, detector, and controller, is able to perform an experiment from start to finish with all standard laboratory functions incorporated. Each of these microstructured components is also developed and used separately. Today, there is a variety of micro -reactors, -contactors, -extractors, and -separators with unique designs to meet the specialized application requirements. Unfortunately, their prominent feature is the lack of standardization hindering the path to mass production and commercialization, even though they have proven to be successfully implementable in a range of applications in several areas such as clinical diagnostics, food analysis, environmental analysis, or drug discovery and delivery studies [59].

6 Detection

6.1 Detection of transactinides

Transactinides disintegrate either by alpha decay or spontaneous fission. Alpha decay detectors are used in gas phase chemistry experiments in which they surround the chromatographic column forming "a sandwich". This has multiple benefits. Radioactive compounds deposit directly on the extremely thin detector surface so no preparation of a sample for detection is required, which saves valuable time. Also, the sandwich detector geometry can be approximated as 4π. This was implemented during the gas phase experiment with $Sg(CO)_6$ using COMPACT, a gas thermochromatography column and detector in one, as previously mentioned in chapter 2.2.5. Detection of alpha decay is also possible in liquid phase experiments, although it has a few drawbacks. The samples for detection have to be prepared by evaporation of a liquid volume. Although automated on-line detection systems coupled with a liquid chemistry system exist (e.g. AIDA in chapter 2.2.4), the process is time consuming and allows only 2π geometry detection. This is caused by the foil the sample is deposited onto, which is too thick for detection of particles α. Alpha detectors are also used for spontaneous fission events detection. The spontaneous fission debris, heavy and highly charged, act like an enormous alpha particle. Fission fragment track detectors are also used.

6.2 Detection of homologs of transactinides

For molybdenum, specifically the isotope ^{99}Mo was studied. It is a 100% β^- emitter as it transforms to its daughter nucleus ^{99m}Tc. ^{99m}Tc undergoes internal conversion in 99,99 % of the decays, during which a shell electron, characteristic roentgen radiation, and auger electrons are emitted. Both nuclides have detectable gamma lines [60].

Tungsten isotopes created in the nuclear reaction of a natural Hf target with ^3He projectiles reside above the river of stability in a nuclide chart making them β^+, EZ, and γ emitters (if not stable, e.g. $^{180,182,183}W$) [60]. Positrons from β^+ decay provide an annihilation peak at 511 keV. Unfortunately, this specific peak is not helpful in a mixture of positron emitters.

In all cases, gamma radiation will be the most convenient to detect. Instruments that use a solid material to detect gamma radiation can be divided into two following groups: inorganic scintillators and semiconductor detectors.

An inorganic scintillation counter usually contains a monocrystal, which may need to be activated via an activator that provides additional energy bands. Such material absorbs the gamma or high energy roentgen radiation and undergoes a luminescence process: electrons in the crystal valence band get excited (or even ionized) to excitation (or in case of ionization to conduction) band and de-excite back by scintillation photon emission. The photons are of discreet energies that reside in the UV-Vis area of the electromagnetic spectrum, but the number of them is directly proportional to the energy of the deposited photon. The scintillation photons are led by photoconductors into a photomultiplier, which is an electronic component consisting of a photosensitive cathode, a set of dynodes and an anode. On the photocathode, the conversion of scintillation photons to electrons takes place taking advantage of the photoelectric effect. These photoelectrons are further accelerated and exponentially multiplied by a set of dynodes forming an electric current impulse that hits the collector anode. The electronic output signal is then further processed and analyzed. Concerning its properties, it has a higher detection efficiency, but shortfalls regarding energy resolution [61], [62].

Semiconductor detectors are sometimes referred to as diode detectors and they indeed work as a large diode in reverse bias connection. In this setup, application of high voltage onto the diode is only safe if no charge carriers are present, otherwise the introduced breakdown current damages the diode permanently. At room temperatures many electrons reside in the conduction band as they are easily thermally produced. To limit thermal excitation, and thus prevent instrumental damage, semiconductor detectors have to be cooled either with liquid nitrogen or electrical coolers. After these measures are taken, high voltage can be applied and depletion region is created. The depletion region is also the area for radiation detection. The ionizing particle excites the electrons from the valence to conduction band and an electron-hole pair is created. The number of pairs is directly proportional to the energy of the deposited particle. Electrons and holes transit to their respective electrode, where they are collected and an electronic output signal is formed. These detectors have several times worse detection efficiency than scintillator detectors but exhibit excellent energy resolution that is not matched by any other type of detector. As a result, they are well suited for spectrometry works [62], [63].

7 Experimental part

7.1.1 List of chemicals

Name (formula), manufacturer (purity):

Sodium chloride (NaCl), Lachner (p.a.)

Ammonium hydroxide (NH_4OH), Penta (25%, p.a.)

Nitric acid (HNO_3), Sigma-Aldrich (≥ 65%)

Sodium nitrate ($NaNO_3$), Lachema (p.a.)

Cyanex® 600, Cytec (Solvay) (≥ 95%)

Kerosene, Sigma-Aldrich (reagent grade)

Octanol ($C_8H_{18}O$), Sigma-Aldrich (≥ 99%)

Ultra Technekow FM $^{99}Mo/^{99m}Tc$ generator, Curium Pharma

7.1.2 List of equipment and supplies

Glass beakers, glass volumetric flasks

5-ml plastic vials, Eppendorf

4-ml HDPE scintillation vials, Kartell

5-ml PP test tubes with caps for phase contacting and separation, Simport

Automatic Research Plus pipettes and pipette tips (100-1000µl), Eppendorf

ZX Classic Vortex Mixer, VELP Scientifica

Centrifuge EBA20, Hettich Zentrifugen

Analytical balance APX-200, Denver Instruments

FEP and PTFE capillaries, inner diameter 250 µm, Dolomite Microfluidics

Glass micromixer chips, Dolomite Microfluidics

PVDF hydrophobic Durapore membrane filter (25mm diameter and 0.22 µm pore size), Merck Millipore

Mitos Duo XS Basic Syringe Pumps, Dolomite Microfluidics

Single-channel analyzer NV 3102 coupled with a well-type detector NaI:Tl, TESLA

Multi-channel analyzer coupled with a semiconductor 45% GEM HPGe detector, ORTEC

Spectra analysis software MAESTRO 7.01, ORTEC

Cyclotron U-120M (provided by ÚJF AV ČR)

7.2 Characterization of the chemical system

The seaborgium homolog ^{99}Mo was obtained by elution of a ^{99}Mo/^{99m}Tc medicinal radionuclide generator with a 3M NH_4OH solution [34].

The aqueous phase consisted of varied concentrations of HNO_3 in *p*H range from -0.3 up to 2.0, where each of them was increased by an increment of 0.03 mol L^{-1} to counteract the 100 μL spiking solution of ^{99}Mo in 3M NH_4OH added to 10 ml of the acidic solution. In the first experiment, the influence of concentration of nitrates has not been studied yet, thus calculated additions of $NaNO_3$ were also a part of the aqueous solution to keep the nitrates at a constant concentration of 2 mol L^{-1}. In later experiments, controlling the nitrate levels was deemed unnecessary.

For the organic phase, kerosene (a liquid mixture of C10-C16 hydrocarbon chains) was used as the solvent in combination with octanol, an inhibitor of third-phase formation (foam), occupying 1 % of the organic phase volume. As an extracting agent, the essential component of the system, Cyanex® 600 was used in concentrations given for the specific experiments in the range from 0.007 to 0.7 mol L^{-1}.

For experiments with tungsten, a cyclotron-produced mixture of tungsten nuclides was deposited onto a glass-microfiber filter, from where they were acquired by washing the filter with HNO_3 of the concentration of choice for the experiment. In comparison to ^{99}Mo, the addition of 0.03 mol L^{-1} HNO_3 did not have to be introduced to the aqueous phase.

7.3 Methodics used in the experiments

The setup for (semi)on-line separation experiments involving cyclotron-produced radionuclides begins with an isochronous cyclotron U-120M (provided by ÚJF AV ČR). The U-120M cyclotron is a particularly universal and tunable device of its kind and accelerates a wide variety of particles such as p^+/H^-, D^+/D^-, $^3He^{+2}$ and $^4He^{+2}$. [64] For our purposes, $^3He^{+2}$ was chosen as a suitable projectile in combination with a hafnium target of natural composition. Projectiles with energy of 50 MeV were used and the average beam intensity was around 300 nA. See

Fig. *10* for better orientation. The nuclear reaction takes place in a target chamber and results in recoiled nuclei that are collected onto KCl aerosol particles carried by ^{4}He gas-jet stream. This is the so-called gas-jet transport technique. The aerosol particles are generated beforehand in a tube furnace containing powdered KCl. The furnace has to induce a controlled temperature of at least 650 °C for an effective evaporation of KCl to take place [65]. A gas cylinder acts as a source of the carrier helium gas, which is additionally looped in the system. From target chamber, the radioactivity-loaded aerosols are led to

be collected on a filter. After a given collection time, the filter is dissolved in a selected aqueous phase. The direct-catch technique is currently utilized for manual batch liquid-liquid extractions.

Nevertheless, the development of an on-line preparation of a liquid sample and consequent chemical processing is already in motion. A hopeful proposal of such a system is illustrated in Fig. 10.

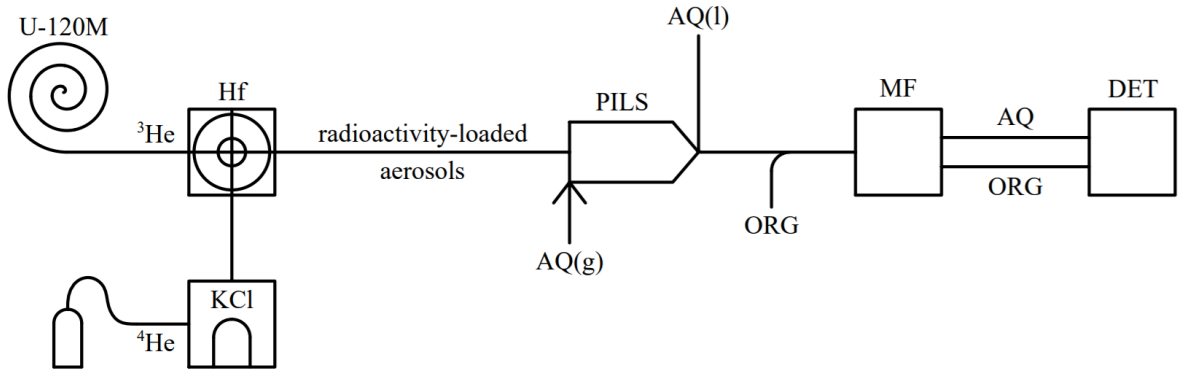

Fig. 10: Schematic of the proposed experimental setup for on-line separation of cyclotron-produced homologs of transactinide elements.

The common batch technique was performed, where 1 ml of spiked aqueous phase was transferred to a long vial containing 1 ml of organic phase. Since kinetics of ^{99}Mo extraction in this particular chemical system was already studied [66], it can be stated with certainty, that by vortex-mixing of the phases for 15 min at 2500 rpm, equilibrium is established. Subsequently, the phases were separated by 1 min of centrifuging at 6000 rpm. A sample of each phase, 800 µl, was taken to be measured on a detector.

For the microfluidic experiments, composition of the aqueous and organic phases was kept the same. The difference between batched manual and microfluidic extractions lies in the continual conduct. The flow rates are determined by piston pumps, which are controlled via a computer. Time of contact has to be later calculated from the flow rate and the total volume taken up by both phases between the point of in-mixing and separation. This total volume constitutes of the volume of the mixer, half of the volume of the separator and the volume of the capillary connecting them. After separation in a hydrophobic membrane-based separator, each of the phase-dedicated capillaries lead the fluids to a waste-collection vial (aqueous phase) or pump piston cylinder (organic phase). To collect the aqueous phase sample, a miniature Eppendorf vial was inserted into the waste-collecting vial.

For organic phase, the volume of the pump cylinder is simply emptied into the sample vial. The sample volumes vary in a range from 150 to 200 µl. Finally, all samples were measured.

The liquid-liquid extraction technique leads to **detection** of liquid samples in plastic vials. This provides consistency regarding detection geometry if measured volumes are kept consistent. Overall, two detectors were used – a scintillation counter and a semiconductor detector. Specifically, the scintillation counter used contains a NaI crystal doped with thallium and is coupled with a single-channel analyzer. This detector is the better choice for samples that contain less radioactivity (e.g. when the distribution ratio *D* is particularly high or low). What contributes to a higher number of registered disintegrations is actually a list of effects:

- high detection efficiency of the detector
- integral registration of the counts,

and what more than doubles the result,

- registration of the mother and daughter nuclide disintegration at the same time, which is possible thanks to the transient equilibrium (both decrease at the same rate – the half-life of the mother nuclide).

Measurement could only be carried out after waiting for approximately ten half-lives of the daughter nuclide for the equilibrium to be established. This approach would however not be applicable in cases where absolute radioactivity would be sought for.

Except for the first experiment, all samples from subsequent experiments expressed sufficient amounts of radioactivity, hence a semiconductor detector was used. Precisely, it was a HPGe (High Purity Germanium) detector coupled with a multi-channel analyzer that allows gamma spectrometry to be conducted.

The spectra analysis software MAESTRO 7.01 was applied. In the case of ^{99}Mo, the 141 keV peak with intensity (89 ± 4) % originating from ^{99m}Tc was selected, the second-best choice would be the peak of energy 181 keV and intensity (6.05 ± 0.12) % from ^{99}Mo (Fig. 11Fig. 12) [67], [68]. Using the peak corresponding to ^{99m}Tc is absolutely permissible, since after the transient equilibrium is reached, the ratio between mother (^{99}Mo) and daughter nuclide (^{99m}Tc) radioactivities is constant.

For the cocktail of cyclotron-produced nuclides of tungsten, using the HPGe detector was a necessity, as a specific nuclide had to be chosen to be measured. The peak of choice happened to be at 100 keV with relative intensity 1816 % provided by ^{176}W, a nuclide with a 2.5h half-life (Fig. 14) [69]. Special attention was paid to which peak to consider, because lots of peaks present are actually double-peaks (two distinct peaks overlapping). They can be identified by being skewed (Fig. 14).

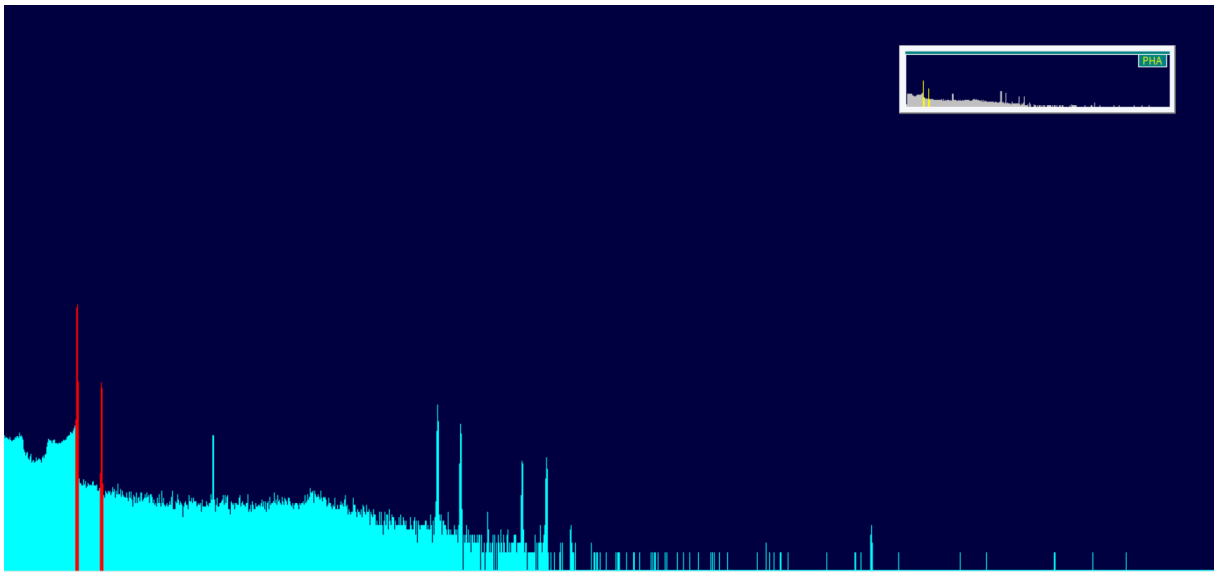

Fig. 11: Spectrum in the range of 13–2050 keV with highlighted peaks 141 keV from ^{99m}Tc and 181 keV from ^{99}Mo.

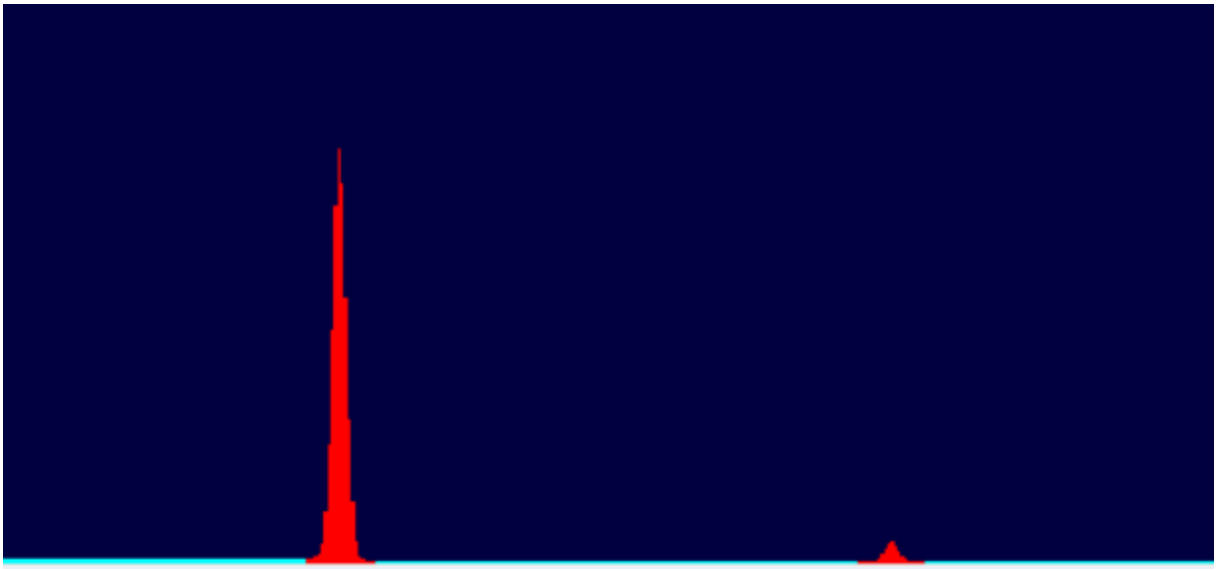

Fig. 12: A zoom of the previous spectrum illustrating the ratio between the peaks 141 and 181 keV.

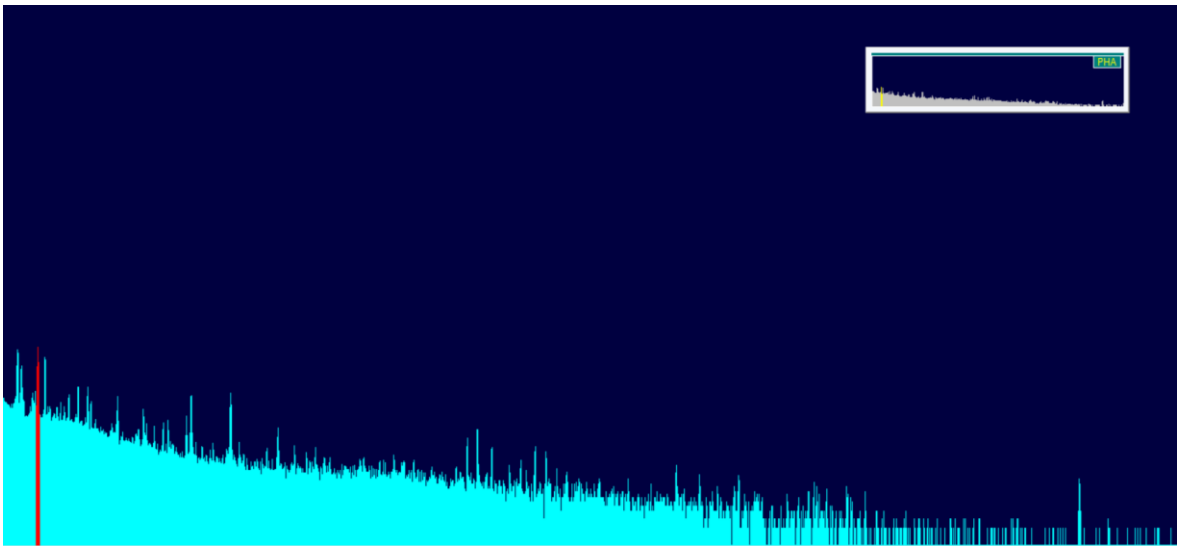

Fig. 13: Spectrum in range of 15–2050 keV with a highlighted peak 100 keV from ^{176}W

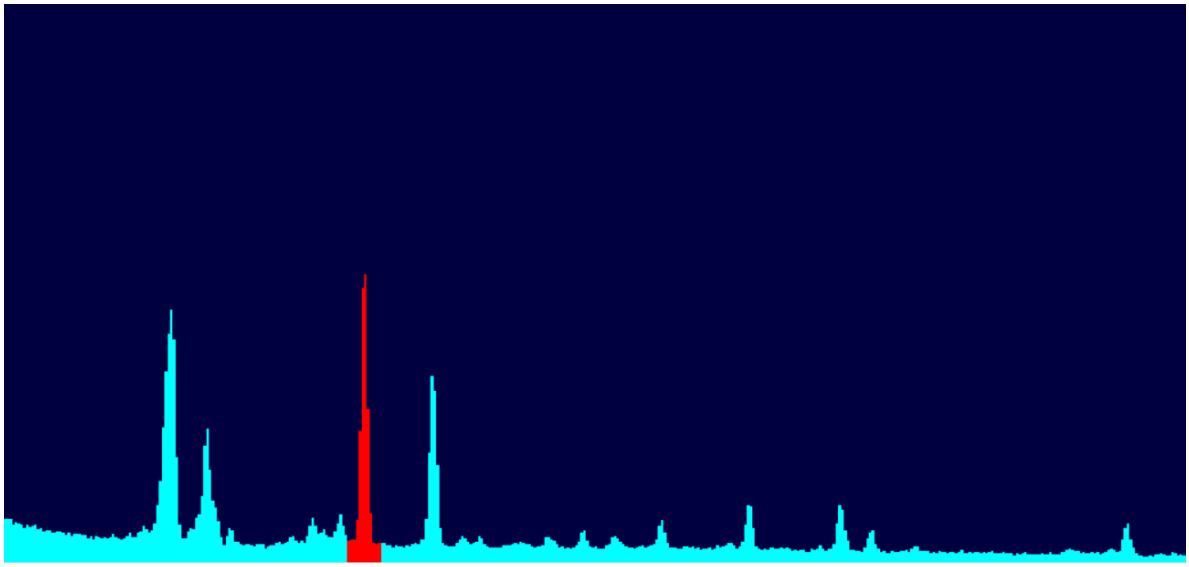

Fig. 14: A zoom of the previous spectrum (c. 20–280 keV) with a highlighted peak 100keV surrounded predominantly by double-peaks.

7.4 Calculations and statistics

Spectrometrically acquired peaks are histograms spanning over *n* channels with counts dispersed following the Gaussian distribution. The peak area constitutes of *gross area* (*GA*), *net area* (*NA*), and *background* (*B*). The relation between these is following:

$$NA = GA - B. \tag{16}$$

The software MAESTRO automatically provides additional information, such as *errors of gross and net area*. Other essential information is detection time t_d (for how long the sample was measured) and *time of measurement* (when the sample was measured) required for decay correction:

$$NA = NA_0 \cdot 2^{-\frac{t}{T}}, \tag{17}$$

where:

NA_0 net area at time t_1
NA net area at time t_2
t time elapsed between t_1 and t_2
T half-life of the analyzed nuclide.

Additionally, the volume of the samples has to be known. With this knowledge, the distribution ratio *D* can be calculated as:

$$D = \frac{NA_{org} \cdot V_{aq} \cdot t_{d,aq}}{NA_{aq} \cdot V_{org} \cdot t_{d,org}}. \tag{18}$$

Radioactive decay is a statistical process inherently carrying a statistical error, which has to be considered whenever involved in further calculations. The Gaussian uncertainty propagation law for the general function $f = f(x_i)$ says that the error of the function *f* equals:

$$\sigma(f) = \sqrt{\sum \left(\frac{\partial f}{\partial x_i}\right)^2 \cdot \sigma(x_i)^2}. \tag{19}$$

Then, the error of D equals:

$$\sigma(D) = \sqrt{\left(\frac{V_{aq} \cdot t_{d,aq}}{NA_{aq} \cdot V_{org} \cdot t_{d,org}}\right)^2 \cdot \sigma\left(NA_{org}\right)^2 + \left(-\frac{NA_{org} \cdot V_{aq} \cdot t_{d,aq}}{{NA_{aq}}^2 \cdot V_{org} \cdot t_{d,org}}\right)^2 \cdot \sigma(NA_{aq})^2} \tag{20}$$

The error of log*D* values are as follows:

$$\sigma(logD) = \sqrt{\left(\frac{1}{D \cdot ln10}\right)^2 \cdot \sigma(D)^2}. \tag{21}$$

The comparison to detection limit values D_{min} and D_{max} was implemented with them being expressed as:

$$D_{min} = \frac{L_{c,org} \cdot V_{aq} \cdot t_{d,aq}}{NA_{aq} \cdot V_{org} \cdot t_{d,org}} \tag{22}$$

$$D_{max} = \frac{NA_{org} \cdot V_{aq} \cdot t_{d,aq}}{L_{c,aq} \cdot V_{org} \cdot t_{d,org}} \tag{23}$$

with critical value L_c

$$L_{C_i} = \frac{\mu}{2}\sqrt{(GA_i - NA_i) \cdot 2 \cdot (n-2)}, \tag{24}$$

where μ is the quantile of the standard Gaussian distribution for 95th percentile [70].

In microfluidic experiments, the time of contacting of the phases is calculated from the flow rate set for the pumps and the volume occupied by contacting phases. It is important to remember that the flow rate doubles (ideally) when both phases meet in the capillary.

Then time of contact for the two phases before being separated is:

$$t = \frac{\frac{V_{mixer}}{2} + V_{capillary} + \frac{V_{separator}}{2}}{2 \cdot flow\ rate}. \tag{25}$$

7.5 Results and discussion

7.5.1 Distribution ratio D dependency on pH for Mo

First of all, dependency of the distribution ratio *D* on *p*H for extraction of molybdenum was observed. This dependency can be seen on Fig. 15. The experiment was performed for five *p*H values (see Tab. 2) with Cyanex 600 concentration of 0.5 mol L^{-1}, which was chosen based on previous experiments [71]. Molar concentration of 2 mol L^{-1} for nitrates has been kept constant. A single channel analyzer with a scintillator detector was used for measurement of the radioactivity of the samples.

Tab. 2: Nitric acid concentrations with corresponding pH values used in the experiment.

c_{HNO_3} [mol L^{-1}]	2.00	1.00	0.50	0.10	0.01
*p*H [-]	-0.30	0.00	0.30	1.00	2.00

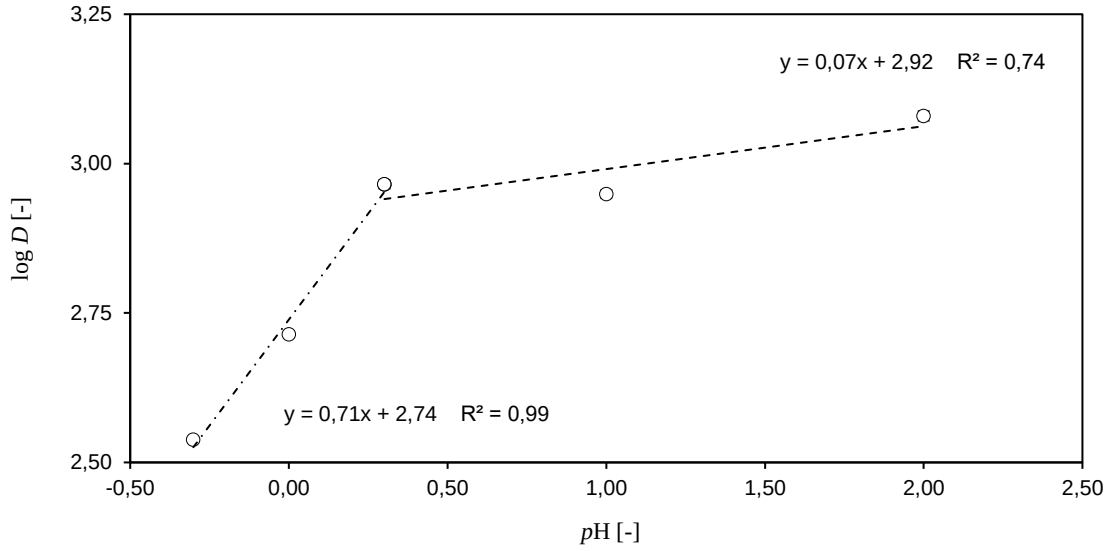

Fig. 15: Log D dependency on pH for extraction of ^{99}Mo with 0.5M Cyanex 600 fitted with two partial linear trendline functions.

Regarding Fig. 15, the maximum of the function is expected to be in the *p*H range of 1 to 2 (we can assume there is a slight drop in the graph due to an outlier point at *p*H = 1.00). Hence, when fitting the plateau area with a linear trendline, the slope should be close to zero (0.07). This is the *p*H range at which neutral species $MoO_2(OH)_2$ are suspected to be extracted, as their extraction is independent of *p*H and no protons are released or consumed during the process.

Left to this plateau, in higher acidity, cationic species like $MoO_2(OH)^+$ and MoO_2^{2+} are being extracted. The first three points were fitted with a trendline with a slope of 0.71 suggesting involvement of an extraction process with one hydrogen released per one molybdenum atom extracted, which hints at extraction of the $MoO_2(OH)^+$ species. To the right of this graph, in lower acidity, extraction of anionic species should occur.

Overall, this figure seems to mirror the findings of other authors using similar extractants at similar concentrations. Quite counter-intuitively, if this experiment was to be repeated, expansion towards higher acidity (lower *p*H) would be beneficial. Although we see a decrease in extractability towards lower *p*H in this graph, the tendency is expected to reverse and a big increase could be discovered [54]. For purposes of seaborgium extraction, the *p*H range of interest would be approximately from 1.00 to 2.00 as the *D*-values reach the maximum there. As mentioned above, in this region neutral species will be extracted, of which there is only one – $SgO_2(OH)_2$.

7.5.2 Distribution ratio *D* dependency on extractant concentration for Mo

The dependency of distribution ratio for extraction of molybdenum was observed for five extractant concentrations at three different *p*H values (Tab. 3) yielding 15 experimental data points and 3 experimental functions (Fig. 16). A single channel analyzer with a scintillator detector was used.

Tab. 3: Nitric acid concentrations with corresponding pH values and Cyanex 600 concentrations with their logarithmic values used in the experiment.

c_{HNO_3} [mol L^{-1}]	1.00	0.50	0.10		
*p*H [-]	0.00	0.30	1.00		
c(Cy) [mol L^{-1}]	0.07	0.10	0.20	0.50	0.70
log *c*(Cy) [-]	-1.15	-1.00	-0.70	-0.30	-0.15

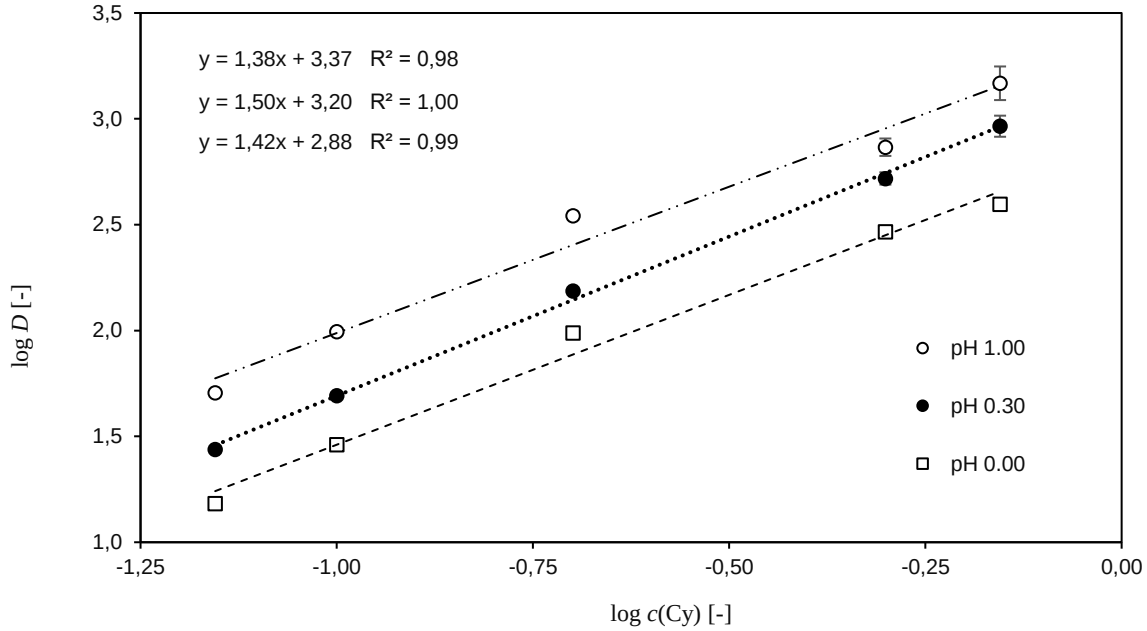

Fig. 16: Log D dependency on extractant concentrations for extraction of molybdenum for 3 pH values each fitted with a linear trendline function

Comparing Fig. 15 and Fig. 16, a definite trend of better extraction with higher *p*H shows. A linear fitting of the three experimental data series plotted a function with non-integer slope values. This either hints at a more complicated extraction mechanism, where 1 molybdenum atom is extracted either by 1 or 2 molecules of the extractant (averaging at the slope values per 1 extracted atom), or the concentration range of the extractant to be "fitted" was not chosen optimally. The latter possibility was experimentally challenged and proved by expanding the extractant concentration range to lower concentrations. By this approach, the slope values have risen up to an integer of 2. In Fig. 16 at higher concentrations of the extractant, a possible plateau is already beginning and skewing the linear trendline [71].

7.5.3 Influence of nitrates on the extraction of Mo

Experiments to reveal the influence of nitrates on the extraction of Mo have been performed in the environment of 0.1M HNO_3 and two concentrations of Cyanex 600 (0.07 mol L^{-1} and 0.5 mol L^{-1}). A weighted amount of $NaNO_3$ powder was added to reach total nitrate concentrations given in Tab. 4. Measurement was carried out on a HPGe detector.

Tab. 4: Concentrations of nitrates with corresponding logarithmic values for extraction of ^{99}Mo from 0.1M nitric acid with 0.07M and 0.5M Cyanex 600.

$c(NO_3^-$, tot) [mol L^{-1}]	0.50	1.00	1.30	1.70	2.00
log $c(NO_3^-$, tot) [-]	-0.30	0.00	0.11	0.23	0.30

The minimum distribution ratio D_{min} values were determined for extractions performed with 0.07M Cyanex 600. The calculated distribution ratios D for two data points (with arrows) are lower than the detectable limit D_{min}. These points were excluded from the linear regression fitting below in Fig. 17:

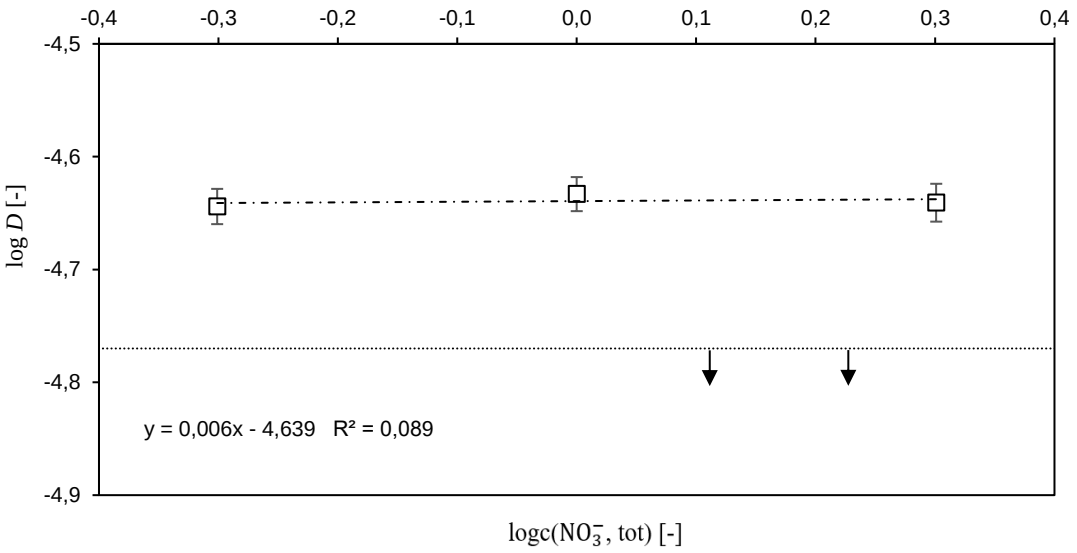

Fig. 17: Log D dependency on concentration of nitrate anions in 0.1M HNO_3 and 0.07M Cyanex 600 with excluded values below detectable limit (arrows) and rest of the values fitted with a linear trendline.

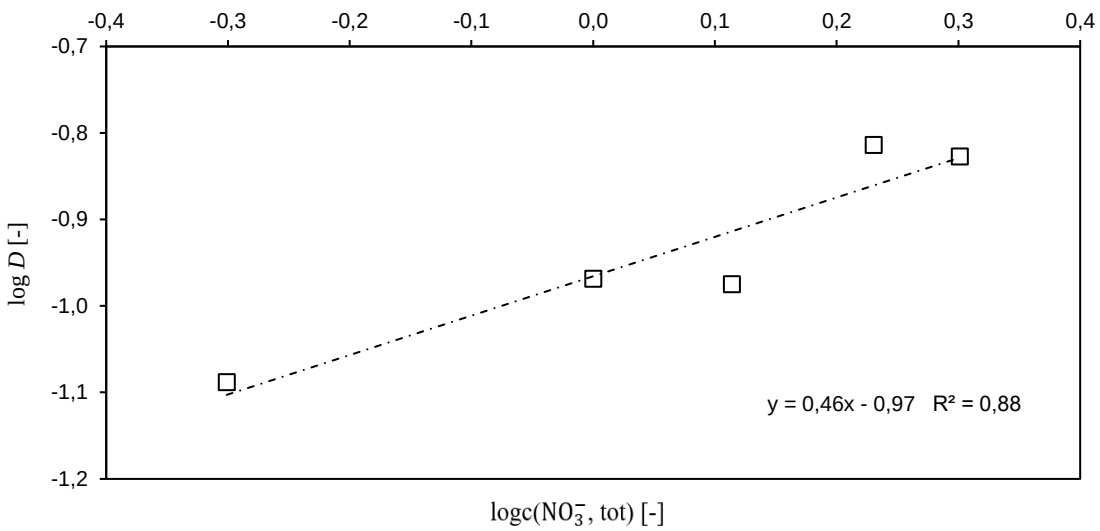

Fig. 18: Log D dependency on concentration of nitrate anions in 0.1M HNO_3 and 0.5M Cyanex 600 fitted with a linear trendline.

In both Fig 17 and Fig. 18, the ideal value for a slope would be 0. A zero value would mean that no influence on extractability of molybdenum within this specific chemical system has been found. The slope in Fig. 17, where Cyanex 600 concentration was 0.07 mol L^{-1}, is satisfyingly close to zero, however, its reliability is disputable. The more reliable looking Fig. 18 with 0.5M Cyanex 600 shows a slope close to 0.5. This means nitrates contribute to molybdenum extraction possibly by the extraction mechanism of ionic associate formation, which occurs only in rather very acidic environment (> 1 mol L^{-1}) and/or in the presence of sufficient nitrate concentration [54]. The nitrate contribution to extraction by chelate formation is however negligible for the experiments and from now on the correction for nitrate anion concentration will no longer be performed.

7.5.4 Distribution ratio *D* dependency on extractant concentration for W

Analogical experiments as with molybdenum were performed with tungsten with four concentrations of nitric acid and five concentrations of Cyanex 600 listed in Tab. 5. The nitrate levels were not accounted for. Samples were measured on a HPGe detector.

Tab. 5: Nitric acid concentrations with corresponding pH values and Cyanex 600 concentrations with their logarithmic values used in the experiment with tungsten.

c_{HNO_3} [mol L^{-1}]	2.00	1.00	0.50	0.10	
*p*H [-]	-0.30	0.00	0.30	1.00	
c(Cy) [mol L^{-1}]	0.007	0.01	0.07	0.10	0.20
log*c*(Cy) [-]	-2.15	-2.00	-1.15	-1.00	-0.70

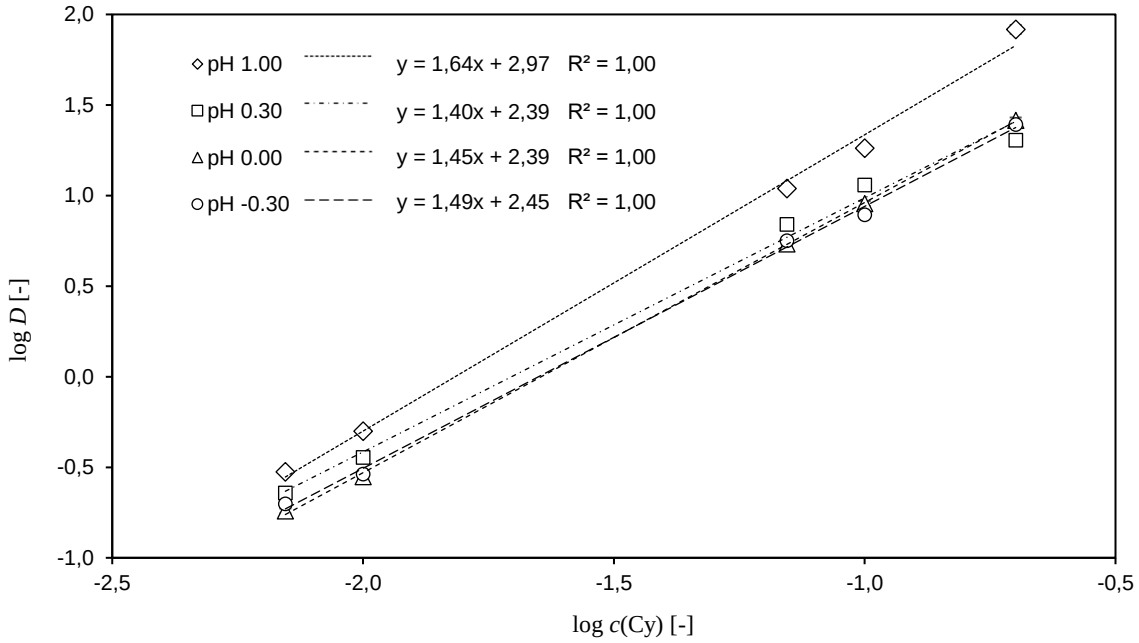

Fig. 19: Log D dependency on extractant concentrations for extraction of W for 4 pH values each fitted with a linear trendline function.

The Fig. 19 confirms all trivial predictions – mirroring Mo, higher *p*H and higher concentration of the extractant provide higher *D*-values. Also the slopes are of similar values and thus similar extraction mechanism is predicted. A yet unobserved effect can be seen in the region of lower *p*H, where a change in *p*H does not induce proportional change in *D*-values.

By combining data from Fig. 16 and Fig. 20, Fig. 20 was created for comparison between Mo and W for Cyanex 600 concentrations in Tab. 6. Better extractability of Mo is apparent. We can see that the slopes, compared to the figures these points were taken from, have increased. The increased values are closer to the expected value of 2: two Cyanex 600 molecules extracting one metal ion. This illustrates how the choice of fitted data points can dramatically change the slope and subsequential interpretation. To be the most accurate, only the points belonging to the linear part of the slope should be fitted. To make a good judgement, more data in a wider range of extractant concentrations have to be acquired.

Tab. 6: Cyanex 600 concentrations with their logarithmic values used to compare extractability of Mo and W.

c(Cy) [mol L^{-1}]	0.07	0.10	0.20
log c(Cy) [-]	-1.15	-1.00	-0.70

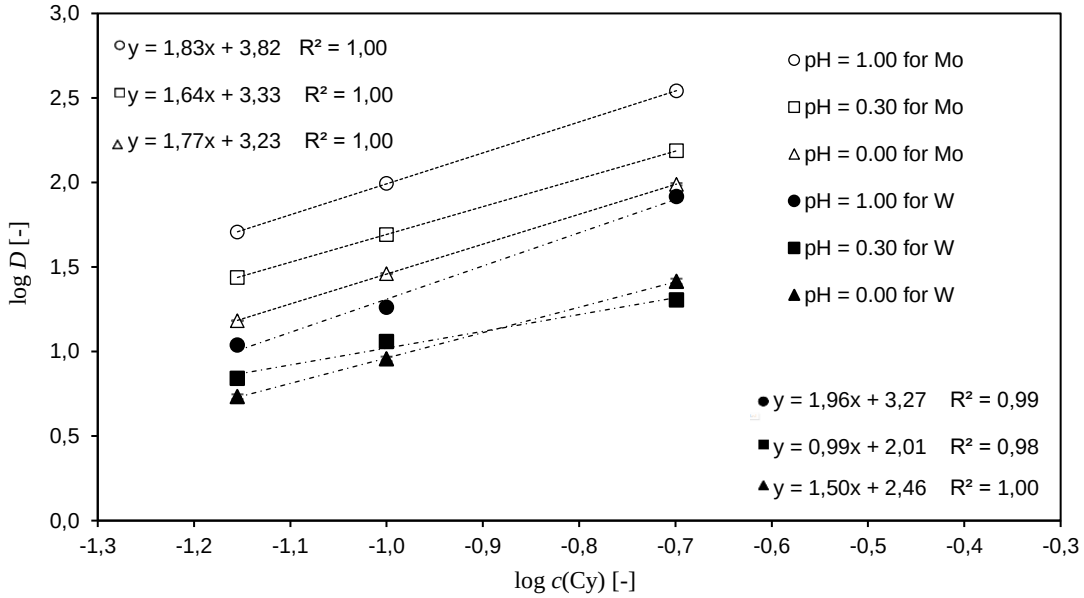

Fig. 20: Log D dependency on extractant concentrations for extraction of Mo and W for 3 pH values each fitted with a linear trendline function.

7.5.5 Kinetics of Mo extraction using microfluidics

For the microfluidic extractions, the composition of the organic phase was kept constant at 0.5M Cyanex 600 concentration. The aqueous phase was varied in terms of acidity provided by HNO_3 (Tab. 7). The experimental series performed with 0.1M HNO_3 was repeated once, resulting in a total of five runs. Each experimental run was carried out for five increasing flow rates (Tab. 8). The acquired values of a logarithm of distribution ratios depending on time of contact are plotted in Fig. 21. The flow rate for the pump at the end of the fluid route was set to be 120 % of the flow rate at the start. These particular values for flow rates were chosen based on the desired flow pattern (segmented flow) in a capillary. The flow rate in a capillary, in which the two phases contact, is double the value of the set flow rate. The flow patterns for each flow rate were observed using a microscopic camera (Fig. 22).

Tab. 7: Nitric acid concentrations with corresponding pH values used in the experiment.

c_{HNO_3} [mol L^{-1}]	2.00	1.00	0.50	0.10
*p*H [-]	-0.30	0.00	0.30	1.00

Tab. 8: Set flow rates, end pump rate, flow rate in the capillary (contact flow rate), and calculated time of contact of the aqueous and organic phase.

flow rate [µl min^{-1}]	200	100	70	30	20
end pump rate [µl min^{-1}]	240	120	84	36	24
contact flow rate [µl min^{-1}]	400	200	140	60	40
time of contact [s]	4	7	11	25	37

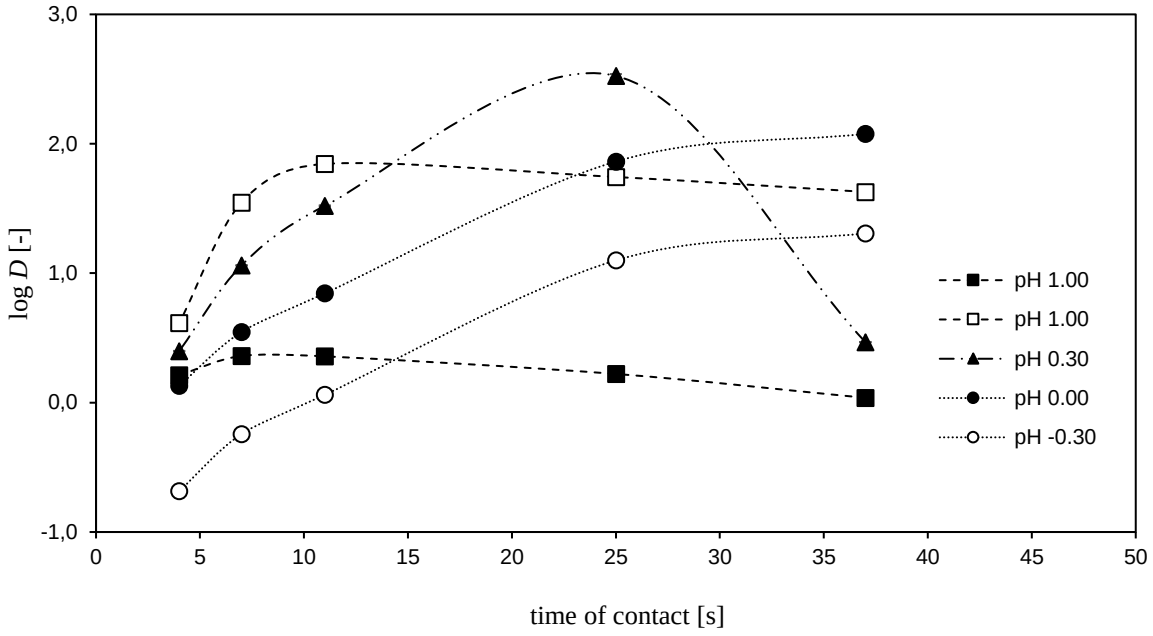

Fig. 21: Log D dependency on flow rates in the microfluidic system for 4 pH values, pH = 1.00 was performed twice. Data points are connected with automatically generated smooth lines for easier readability.

In Fig. 21, we can see a hint of a trend of improved extractability of molybdenum with higher *p*H with the exception of the first measurement (■). Due to the character of microfluidic systems, this was a to-be-expected phenomenon. The system probably has not been saturated with the fluids sufficiently and dead volumes have not been filled yet. It can be assumed that some activity has been lost this way, especially since the experiment was performed starting at the lower values of flow rates, where the deviation is the most prominent. The second run of *p*H 1.00 (□) has been performed last.

The best result was achieved with the flow rate of 60 µl min^{-1} (time of contact 25 s) for *p*H 0.30 (▲). This is surprising since both of these values are not the extremes. Higher *p*H, as was shown in all previous experiments, should theoretically yield better results, as well as prolonging the time of contact should have provided, in general, higher *D*-values. The time of contact seemed to have a continuing positive influence only for the two most acidic runs (●○). Speculation can be conducted about the reliability of both of the pH 1.00 runs and the 37-s ▲ pH 0.30 point. The experiment needs to be repeated with focus on precautionary measures against such deviations, e.q. repeated sampling and thorough washes between solution changes.

It can safely be stated that the fastest flow of 400 µl min^{-1} provides the least efficient conditions for extraction as the time of contact (4 s) is too low. However, in the context of application on Sg, this would be the preferred setting (4 s at □ pH 1.00). The time of contact is low enough, whilst the D-value remains sufficient.

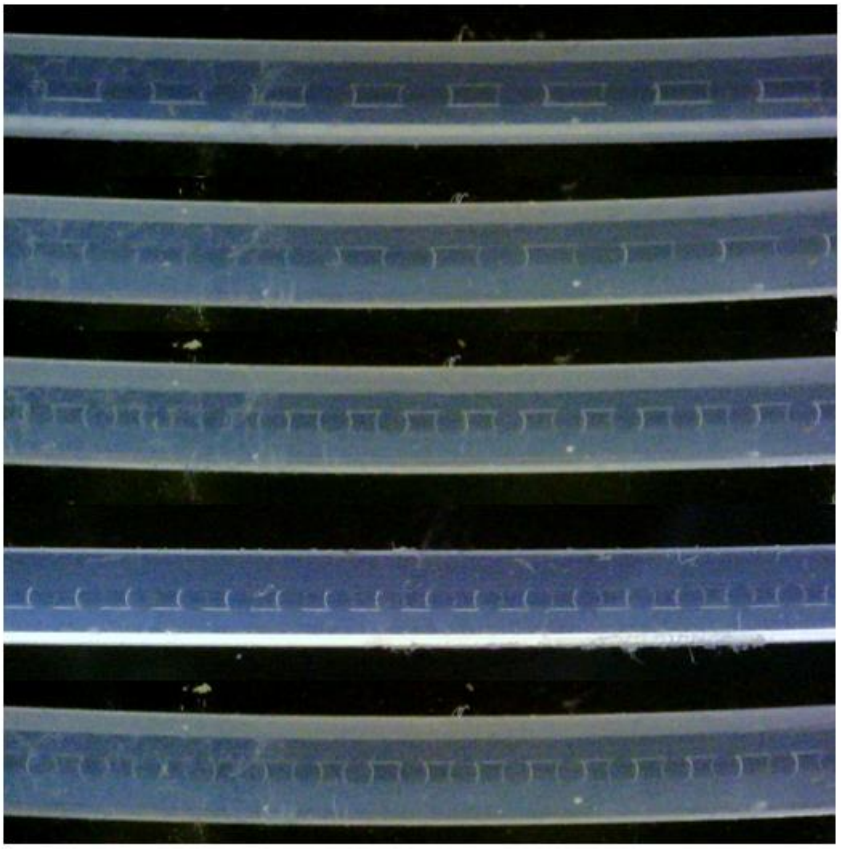

Fig. 22: Flow pattern changes in a segmented flow acquired for flow rates of (top to bottom): 40, 60, 140, 200 and 400 $\mu l\ min^{-1}$.

During the microfluidic experiments, flow pattern was microscopically observed and photographed for more thorough data processing in the future. Recorded flow patterns are depicted in Fig. 22, where it is apparent that the size of the plugs is inversely proportional to the flow rate. Interestingly, in-between the discreet flow rates mentioned above, there has been values that did not provide a segmented flow. No connection between different flow rates and ability to form segmented flow has been observed.

8 Conclusion

In the theoretical part of this work, synthesis of the superheavy elements was described and the problematics regarding their handling was discussed. An overview of apparatuses used for chemistry of transactinides in gaseous and aqueous phase was made. Focusing on seaborgium, its synthesis and chemistry in gaseous and aqueous phase was researched. The chemistry of the homologs of seaborgium was introduced followed by description of a liquid-liquid extraction technique. A few alternative chemical systems for extraction of homologs (and therefore also Sg) were named. The topic of microfluidics was touched upon, debating its characteristics and parameters, advantages, and disadvantages. A quick rundown of detection of transactinides, molybdenum, and tungsten was done.

In the experimental part, a total of five types of experiments were conducted, each giving valuable information. From the experiments, where *D* dependency on *p*H for Mo was investigated, a range of *p*H from 1.00 to 2.00 was providing the biggest *D*-values. In this range, the neutral species $MoO_2(OH)_2$ is extracted. In higher acidities, based on the slope values, species $MoO_2(OH)_2$ and $MoO_2(OH)^+$ are being extracted at the same time. Experiments observing *D*-values based on extractant concentration revealed that most likely 2 molecules of Cyanex 600 extract one metal ion and the *D*-values increase with increased amount of extractant. Nitrates have been found to have a positive effect on ionic associate extraction. From research, this effect becomes apparent only starting at nitric acid concentration > 1 mol L^{-1} or with higher concentrations of nitrates. Both of these conditions do not touch our area of interest, where extraction by chelation applies. After conducting experiments with tungsten, the properties of W and Mo can be proclaimed to be almost identical, with slightly, but clearly, better extractability of Mo. An apparatus for microfluidic experiments has been assembled. During the microfluidic experiments, kinetic experiments with Mo were performed, from which it was apparent that mass transfer was faster for *p*H 1.00, for which equilibrium *D*-values were also the highest. Very basic observation was also made, that with increased contacting time, the *D*-value also grows, however, it was found that even 4-s contacting time is enough to provide *D* equal to 17.2 ± 0.2.

In future experiments expanding both the *p*H and the extractant concentration range would be beneficial in order to gain some perspective. At the current *p*H range, only one local maximum is being observed. It is possible to discover additional maxima, but finding the minima would also be productive, since such information could lead to more accurate identification of the linear parts of the function and thus getting more information about the mechanisms involved in the extraction process. The current extractant concentration range does not show any local extremes. The microfluidic experiments would definitely benefit from repetition as some data points go undeniably against expected trend, which was fully observed in some datasets. With the gained awareness of the proneness to mistakes using this system, precautionary repetitions and washes would be performed.

9 References

[1] S. Wolfram (2015). George Boole: A 200-Year View. https://writings.stephenwolfram.com/2015/11/george-boole-a-200-year-view/ (accessed Aug. 1, 2022)

[2] S. Hofmann et al. (2018). On the discovery of new elements (IUPAC/IUPAP Provisional Report). Pure and Applied Chemistry, vol. 90, no. 11, pp. 1773-1832. https://doi.org/10.1515/pac-2018-0918

[3] IUPAC (2016). IUPAC announces the Names of the Elements 113, 115, 117 and 118. https://iupac.org/iupac-announces-the-names-of-the-elements-113-115-117-and-118/ (accessed Dec. 14, 2021)

[4] IUPAC (2021). IUPAC Periodic Table of the Elements. https://iupac.org/what-we-do/periodic-table-of-elements/ (accessed Dec. 14, 2021)

[5] F. G. Kondev et al. (2021). The NUBASE2020 evaluation of nuclear physics properties. Chinese Physics C, vol. 45, no. 3. https://doi.org/10.1088/1674-1137/abddae

[6] C. E. Düllmann and Michael Block (2018). The Quest for Superheavy Elements and the Island of Stability. Scientific American. https://www.scientificamerican.com/article/the-quest-for-superheavy-elements-and-the-island-of-stability/ (accessed Jun. 20, 2022)

[7] M. Cinausero et al. (2013). Study of binary fragmentation and compound nucleus fission in the reaction 50Ti + 208Pb. Available: http://pos.sissa.it

[8] K. Nishio et al. (2008). Effects of nuclear orientation on the mass distribution of fission fragments in the reaction of 36S + 238U. Physical Review C – Nuclear Physics, vol. 77, no. 6. https://doi.org/10.1103/PhysRevC.77.064607

[9] A. K. Nasirov et al. (2014). Basic distinctions between cold- and hot-fusion reactions in the synthesis of superheavy elements. Physics of Atomic Nuclei, vol. 77, no. 7, pp. 881-889. https://doi.org/10.1134/S1063778814070126

[10] J. Khuyagbaatar et al. (2020). Search for elements 119 and 120. Physical Review C, vol. 102, no. 6. https://doi.org/10.1103/PhysRevC.102.064602

[11] A. Türler and V. Pershina (2013). Advances in the production and chemistry of the heaviest elements. Chemical Reviews, vol. 113, no. 2, pp. 1237-1312. https://doi.org/10.1021/cr3002438

[12] M. Zastrow (2017). In search for “magic” nuclei, theory catches up to experiments. Proceedings of the National Academy of Sciences of the United States of America, vol. 114, no. 20, pp. 5060-5062. https://doi.org/10.1073/pnas.1703620114

[13] P. de Marcillac et al. (2003). Experimental detection of α-particles from the radioactive decay of natural bismuth. Nature, vol. 422, no. 6934, pp. 876-878. https://doi.org/10.1038/nature01541

[14] K. Chapman (2020). The transuranic elements and the island of stability. Philosophical Transactions of the Royal Society A: Mathematical, Physical and Engineering Sciences, vol. 378, no. 2180. https://doi.org/10.1098/rsta.2019.0535

[15] D. C. Hoffman and D. M. Lee (1999). Chemistry of the Heaviest Elements – One Atom at a Time. Journal of Chemical Education, vol. 76, no. 3. https://doi.org/10.1021/ed076p331

[16] M. Leino (2003). Gas-filled separators – An overview. Nuclear Instruments and Methods in Physics Research, Section B: Beam Interactions with Materials and Atoms, vol. 204, pp. 129-137. https://doi.org/10.1016/S0168-583X(02)01901-8

[17] J. V. Kratz (2011). Aqueous-phase chemistry of the transactinides. Radiochimica Acta, vol. 99, no. 7-8, pp. 477-502. https://doi.org/10.1524/ract.2011.1856

[18] M. Kaji (2003). Mendeleev's discovery of the periodic law: the origin and the reception. Foundations of Chemistry 5: pp. 189-214. https://doi.org/10.1023/A:1025673206850

[19] Y. Nagame et al. (2015). Chemical studies of elements with Z≥104 in liquid phase. Nuclear Physics A, vol. 944, pp. 614-639. https://doi.org/10.1023/A:1025673206850

[20] R. Lougheed (1997). Oddly ordinary seaborgium. Nature, vol. 388, pp. 21-22. https://doi.org/10.1038/40272

[21] M. Schädel et al. (1997). Chemical properties of element 106 (seaborgium). Nature, vol. 388, pp. 55-57. https://doi.org/10.1038/40375

[22] M. Schädel (2015). Chemistry of the superheavy elements. Philosophical Transactions of the Royal Society A: Mathematical, Physical and Engineering Sciences, vol. 373, no. 2037. https://doi.org/10.1098/rsta.2014.0191

[23] M. Schädel et al. (1989). ARCA II – A new apparatus for fast, repetitive HPLC separations. Radiochimica Acta, vol. 48, pp. 3-4. https://doi.org/10.1524/ract.1989.48.34.171

[24] D. Hild et al. (2013). MicroSISAK: Continuous liquid-liquid extractions of radionuclides at ≥0.2mL/min. Radiochimica Acta, vol. 101, no. 11, pp. 681-689. https://doi.org/10.1524/ract.2013.2080

[25] H. Persson et al. (1989). SISAK 3 – An improved system for rapid radiochemical separations by solvent extraction. Radiochimica Acta, vol. 48, no. 3-4, pp. 177-180. https://doi.org/10.1524/ract.1989.48.34.177

[26] A. Türler et al. (2015). Chemical studies of elements with Z≥104 in gas phase. Nuclear Physics A, vol. 944, pp. 640-689. https://doi.org/10.1016/j.nuclphysa.2015.09.012

[27] V. Pershina et al. (2021). Reactivity of the superheavy element 115, Mc, and its lighter homologue, Bi, with respect to gold and hydroxylated quartz surfaces from periodic relativistic DFT calculations: A comparison with element 113, Nh. Inorganic Chemistry, vol. 60, no. 13, pp. 9796-9804. https://doi.org/10.1021/acs.inorgchem.1c01076

[28] V. K. Utyonkov et al. (2018). Neutron-deficient superheavy nuclei obtained in the Pu 240 + Ca 48 reaction. Physical Review C, vol. 97, no. 1. https://doi.org/10.1103/PhysRevC.97.014320

[29] M. Schädel et al. (1998). First aqueous chemistry with seaborgium (element 106). Journal of Alloys and Compounds, vol. 271-273, pp. 312-315. https://doi.org/10.1016/S0925-8388(98)00078-4

[30] L. I. Guseva and G. S. Tikhomirova (2002). Ion-exchange procedure developed for isolation of element 106 (seaborgium) and study of its chemistry in H_2SO_4 and H_2SO_4/HF solutions, with W as imitator. Radiochemistry, vol. 44, pp. 337-341. https://doi.org/10.1023/A:1020660508092

[31] J. Even et al. (2014). In-situ formation, thermal decomposition, and adsorption studies of transition metal carbonyl complexes with short-lived radioisotopes. Radiochimica Acta, vol. 102, no. 12, pp. 1093-1110. https://doi.org/10.1515/ract-2013-2198

[32] W. T. Mullins and G. W. Leddicotte (1961). The Radiochemistry of Tungsten. National Research Council. The National Academies Press. https://doi.org/10.17226/21534

[33] J. Barnhart (1997). Occurrences, uses, and properties of chromium. Regul Toxicol Pharmacol, vol. 26, pp. 3-7. https://doi.org/10.1006/rtph.1997.1132

[34] F. M. S. Carvalho and A. Abrao (1997). Sorption and desorption of molybdenum in alumina microspheres. Journal of Radioanalytical and Nuclear Chemistry, vol. 218, pp. 259-262. https://doi.org/10.1007/BF02039347

[35] J. R. de Laeter et al. (2003). Atomic weights of the elements: review 2000. Pure Applied Chemistry, vol. 75, no. 6, pp. 683-800. http://dx.doi.org/10.1351/pac200375060683

[36] J. Magill et al. (2012). Karlsruher Nuklidkarte – Auditorium Chart. Karsruhe: Nucleonica GmbH. JRC75721. ISBN: 978-3-00-036347-4

[37] L. F. Curtiss et al. (1960). The Radiochemistry of Molybdenum. National Research Council. The National Academies Press. https://doi.org/10.2172/4158589

[38] N. D. Betenekov et al. (2016). Influence of molybdenum speciation on its recovery with hydroxide sorbents. Radiochemistry, vol. 58, pp. 63-71. https://doi.org/10.1134/S1066362216010100

[39] V. Pershina and J. V. Kratz (2001). Solution chemistry of element 106: Theoretical predictions of hydrolysis of group 6 cations Mo, W, and Sg. Inorganic Chemistry, vol. 40, no. 4, pp. 776-780. https://doi.org/10.1021/ic0003731

[40] V. Pershina (2004). Theoretical treatment of the complexation of element 106, Sg, in HF solutions. Radiochimica Acta, vol. 92, no. 8, pp 455-462. https://doi.org/10.1524/ract.92.8.455.39279

[41] J. Starý et al. (1975). Separační metody v radiochemii. Academia Praha.

[42] K. Čubová et al. (2018). Extraction of thallium and indium isotopes as the homologues of nihonium into the ionic liquids. Journal of Radioanalytical and Nuclear Chemistry, vol. 318, no. 3, pp. 2455-2461. https://doi.org/10.1007/s10967-018-6270-x

[43] M. F. Attallah et al. (2019). Extractions of carrier-free 99Mo by ionic liquids from acid solutions: a model of seaborgium (Sg) experiment. Applied Radiation and Isotopes, vol. 149, pp. 83-88. https://doi.org/10.1016/j.apradiso.2019.04.020

[44] J. Mendham et al. (2000). Vogel's Quantitative Chemical Analysis, 6th Ed. ISBN: 978-058222628-9.

[45] D. M. Imam and Y. A. El-Nadi (2018). Recovery of molybdenum from alkaline leach solution of spent hydrotreating catalyst by solvent extraction using methyl tricaprylammonium hydroxide. Hydrometallurgy, vol. 180, pp. 172-179. https://doi.org/10.1016/j.hydromet.2018.07.022

[46] L. Karagiozov and C. Vasilev (1979). Separation of molybdenum and rhenium by extraction with mixtures of trioctylamine and aliquat 336 followed by selective stripping. Hydrometallurgy, vol. 4, pp. 51-55. https://doi.org/10.1016/0304-386X(79)90005-7

[47] S. Lahiri and B. Mukhopadhyay (1997). Liquid-liquid extraction of carrier-free radioisotopes produced in α-particle activated molybdenum target by HDEHP and TBP. Elsevier Science Ltd, vol. 48. https://doi.org/10.1016/s0969-8043(97)00017-1

[48] J. Coca et al. (1990). Solvent extraction of molybdenum and tungsten by Alamine 336 and DEHPA. Hydrometallurgy, vol. 25, no. 2, pp. 125-135. https://doi.org/10.1016/0304-386X(90)90034-Y

[49] T. Hirai and I. Komasawa (1990). Separation and purification of vanadium and molybdenum by solvent extraction followed by reductive stripping. Journal of chemical engineering of Japan, vol. 23, no. 2, pp. 208-213. https://doi.org/10.1252/jcej.23.208

[50] N. I. Gerhardt et al (2000). Extraction of tungsten VI, molybdenum VI and rhenium VII by diisododecylamine. Hydrometallurgy, vol. 55, no. 15. https://doi.org/10.1016/s0304-386x(99)00068-7

[51] T. Sato et al. (1990). Liquid-liquid extraction of molybdenum VI from aqueous acid solutions by TBP and TOPO. Hydrometallurgy, vol. 23, pp. 297-308. https://doi.org/10.1016/0304-386X(90)90011-P

[52] Chemical structure of HDEHP https://www.sigmaaldrich.com/CZ/en/product/aldrich/237825?gclid=CjwKCAjw2rmWBhB4EiwAiJ0mtaLP7aPQ7aJYadLXpMqpsh2XRgGJB7BXTzvqf9sfK4aTbBl1PSxcTxoCyxEQAvD_BwE (accessed Jul. 13, 2022)

[53] S. van Roosendael et al. (2019). Recovery of cobalt from dilute aqueous solutions using activated carbon-alginate composite spheres impregnated with Cyanex 272. RSC Advances, vol. 9, no. 33, pp. 18734-18746. https://doi.org/10.1039/c9ra02344e

[54] C. Marie et al. (2016). Behavior of molybdenum VI in {DMDOHEMA-HDEHP/nitric acid} liquid-liquid extraction systems. Solvent Extraction and Ion Exchange, vol. 34, no. 5, pp. 407-721. https://doi.org/10.1080/07366299.2016.1208029

[55] G. M. Whitesides (2006). The origins and the future of microfluidics. Nature, vol. 442, no. 7101, pp. 368-373. https://doi.org/10.1038/nature05058

[56] M. N. Kashid (2011). Gas-liquid and liquid-liquid mass transfer in microstructured reactors. Chemical Engineering Science, vol. 66, no. 17, pp. 3876-3897. https://doi.org/10.1016/j.ces.2011.05.015

[57] D. Liu et al. (2017). A simple online phase separator for the microfluidic mass transfer studies. Chemical Engineering Journal, vol. 325, pp. 342-349. https://doi.org/10.1016/j.cej.2017.05.056

[58] P. F. Jahromi et al. (2017). Pressure-driven liquid-liquid separation in Y-shaped microfluidic junctions. Chemical Engineering Journal, vol. 328, pp. 1075-1086. https://doi.org/10.1016/j.cej.2017.07.096

[59] Y. C. Lim et al. (2010). Lab-on-a-chip: A component view. Microsystem Technologies, vol. 16, no. 12, pp. 1995-2015. https://doi.org/10.1007/s00542-010-1141-6

[60] National Nuclear Data Center. NuDat 3 https://www.nndc.bnl.gov/nudat3/ (accessed Jun. 20, 2022)

[61] T. Yanagida (2018). Inorganic scintillating materials and scintillation detectors. Proceedings of the Japan Academy Series B: Physical and Biological Sciences, vol. 94, no. 2, pp. 75-97. https://doi.org/10.2183/pjab.94.007

[62] F. S. Goulding (1966). Semiconductor detectors for nuclear spectrometry. Nuclear Instruments and Methods, vol. 43, pp. 1-54. https://doi.org/10.1016/0029-554X(66)90531-3

[63] P. Rehak and E. Gatti (1989). State of the art in semiconductor detectors. Nuclear Instruments and Methods, vol. 289, pp. 410-417. https://doi.org/10.1016/0168-9002(90)91511-9

[64] Zkoumání supertěžkých prvků. https://www.3pol.cz/cz/rubriky/fyzika-a-klasicka-energetika/2193-zkoumani-supertezkych-prvku (accessed Jun. 5, 2021)

[65] L. L. Wang et al. (1996). Vacuum evaporation of KCl-NaCl salts: Part II. Vaporization-rate model and experimental results. Metallurgical and Materials Transactions B, vol. 27, pp. 433-443. https://doi.org/10.1007/BF02914908

[66] P. Bartl et al. Fast microfluidic extraction of Sg homologues at new joint CTU, UiO and NPI facility in Řež. Poster from the conference: https://indico.gsi.de/event/8176/

[67] Nuclear data for 99mTc https://www.nndc.bnl.gov/nudat3/decaysearchdirect.jsp?nuc=99TC&unc=nds (accessed Aug. 2, 2022)

[68] Nuclear data for 99Mo
https://www.nndc.bnl.gov/nudat3/decaysearchdirect.jsp?nuc=99MO&unc=nds
(accessed Aug. 2, 2022)

[69] Nuclear data for 176W http://nucleardata.nuclear.lu.se/toi/nuclide.asp?iZA=740176
(accessed Aug. 2, 2022)

[70] I. Obrusník and J. Kučera (1978). The digital methods of peak area computation and detection limit in gamma-ray spectrometry. Radiochemical and Radioanalytical Letters, vol. 32, pp. 149-160.

[71] P. Bartl (2022). Dissertation on Study of Extraction of Transactinide Homologues.